

# Tidally influenced deposits in the Río Alías Strait connecting a marginal basin with the Mediterranean Sea (Pliocene, South-East Spain)

Fernando Sola<sup>1</sup> | Ángel Puga-Bernabéu<sup>2</sup>  | Juan C. Braga<sup>2</sup>

<sup>1</sup>Departamento de Biología y Geología, Universidad de Almería, Almería, Spain

<sup>2</sup>Departamento de Estratigrafía y Paleontología, Universidad de Granada, Granada, Spain

## Correspondence

Ángel Puga-Bernabéu, Departamento de Estratigrafía y Paleontología, Universidad de Granada, Campus de Fuentenueva, Granada 18002, Spain.  
Email: [angelpb@ugr.es](mailto:angelpb@ugr.es)

## Funding information

Consejería de Conocimiento, Investigación y Universidad, Junta de Andalucía, Grant/Award Number: A-RNM-438-UGR20; Ministerio de Ciencia e Innovación, Grant/Award Number: PGC2018-099391-B-100; Consejería de Conocimiento, Investigación y Universidad, Junta de Andalucía, Grant/Award Number: RNM-190

## Abstract

The Río Alías Strait developed in the Early Pliocene as a narrow marine corridor at the connection of the microtidal Mediterranean Sea and the north-eastern margin of the Almería-Níjar Basin in the eastern Betic Cordillera (South-East Spain). The orientation and topography of the strait were controlled by the transpressive Carboneras and Polopos/South Cabrera fault systems. Ten sedimentary facies occur in the up to 150 m thick mixed biogenic carbonate-terrigenous succession distinguished on the basis of their lithology, components, grain size, stratal geometries and sedimentary structures, which were observed in seven sections at well-exposed outcrops of four sectors. The sedimentary record of the Río Alías Strait reflects the morphological constraints, which conditioned its sedimentary dynamics and facies distribution. Even in this microtidal setting, tidal current amplification through narrow constrictions produced thick accumulations of large cross-stratified bodies up to 15 m thick formed by the opposite migration of three-dimensional simple and compound dunes. The Río Alías Strait reconstruction shows: (1) a very narrow constriction in the central sector from which “constriction-related deltas” (CRDs) formed in the flood downstream (westward) and ebb (upstream) directions and (2) a relatively deep depression (>65 m water depth) separating the eastern and central-east sectors, where tidal current energy was attenuated and dunes were not generated. The closure of the strait resulted from the tectonic uplift of the antecedent upland of Sierra Cabrera at the northern side, which promoted the southward progradation of deltaic systems over the strait. The Río Alías Strait represents the only clear record of a microtidal strait in the Betic Cordillera since the Miocene. The case study presented here improves existing models on the sedimentary dynamics of ancient tidal-dominated straits by expanding the knowledge on their spatial environment variability.

## KEYWORDS

Almería-Níjar Basin, large-scale dunes, microtidal regime, mixed siliciclastic-carbonate sediments, sedimentary dynamics, tidal straits

This is an open access article under the terms of the [Creative Commons Attribution](https://creativecommons.org/licenses/by/4.0/) License, which permits use, distribution and reproduction in any medium, provided the original work is properly cited.

© 2024 The Author(s). *The Depositional Record* published by John Wiley & Sons Ltd on behalf of International Association of Sedimentologists.

## 1 | INTRODUCTION

The accurate reconstruction of the palaeogeography and palaeoecology of sedimentary basins interconnected through straits and seaways relies on the understanding of the specific sedimentary dynamics and evolution of these particular depositional systems (Gattolin et al., 2013; Capella et al., 2018; Gardner & Dorsey, 2021; Beelen et al., 2022; Rossi et al., 2023a).

Water circulation and currents in straits can be driven by different processes (Dalrymple, 2023): (1) tides (tidal currents); (2) winds and/or atmospheric-pressure differences (meteorologically generated currents); (3) density differences between interconnected water masses (estuarine and inverse estuarine circulation) and (4) global wind or ocean circulation (oceanic currents). Convergence and constriction of marine waters in straits result in current amplification and acceleration followed by expansion and deceleration at the exits controlling the distribution of sediments (Longhitano, 2013; Dalrymple, 2023). In tidal-dominated straits and regardless of the tidal regime, the periodic movement of water promoted by tidal cycles at different time scales leads to tidal current asymmetry (i.e. currents with opposite directions and variable velocities; Reynaud & Dalrymple, 2012), which generally results in a variety of seabed features common in tide-dominated shelves but with a marked bidirectional transport pathway at regional scale (Longhitano & Chiarella, 2020). Tide-influenced strait deposits form thick (10s to few 100s m) stratigraphic successions that show large-scale cross stratification, erosional discontinuities and tide-related sedimentary features such as tidal bundles (with a general lack of muddy intervals) and herringbone cross strata indicating bidirectional current patterns (Longhitano et al., 2012), which occur in relatively predictive facies tracts aligned along the strait axis (Longhitano, 2013).

The geomorphic constriction needed for strait formation is the result of the geological evolution of the region in which the strait is located (Dalrymple, 2023). Most modern and ancient examples of straits in the Mediterranean Sea are formed by rifting separating emergent land masses in back-arc settings (Cavazza & Longhitano, 2022). The sedimentary features and evolution of Neogene to Quaternary straits connecting subbasins in the western Mediterranean (Cavazza & Longhitano, 2022) show that even within a microtidal sea, such as the Mediterranean, flow constriction in straits might generate tidal-current amplification and clastic dune-bedded deposits (Longhitano, 2013, 2018a, 2018b).

The Neogene Betic straits connecting the Mediterranean Sea with the Atlantic Ocean are among the best-known examples of ancient emergent straits (Martín et al., 2001, 2009, 2014; Betzler et al., 2006; Braga et al., 2010;

Puga-Bernabéu et al., 2022). Instead of developing in rifting settings, they evolved and eventually closed as the Betic Cordillera uplifted in a compressional context caused by the convergence of the African and Eurasian plates (Dewey et al., 1989; Sanz de Galdeano, 1990; Rosenbaum et al., 2002). In this regime, the straits follow elongated grabens produced by local extension related to NW-SE normal faults resulting from the NW-SE directed compression (Galindo-Zaldivar et al., 2019). These straits connected Mediterranean-linked intermontane basins with the Atlantic-linked Guadalquivir Basin, the foreland basin of the cordillera, but they were ways of water interchange between the major water masses of the Mediterranean Sea and the Atlantic Ocean prior to the temporal disconnection that caused the Messinian salinity crisis (MSC; Martín et al., 2014).

In contrast, the Pliocene strait deposits described here accumulated after the MSC (Dabrio, 1987; Aguirre, 1998) in a connection of the intermontane Almería-Níjar Basin with the Mediterranean Sea, the Río Alías Strait (Figure 1). In other words, the strait connected the Mediterranean Sea with one of its marginal basins (Dabrio et al., 1981; Montenat, 1990; Braga et al., 2003). This was a small, narrow strait, 13 km long and with a maximum width of 2 km according to the present-day extension of its deposits. In the north-eastern Almería-Níjar Basin, the sedimentary evolution was conditioned by a left-lateral fault system, the Carboneras Fault Zone (CFZ) (Figure 1). This fault system and the uplift of the Sierra Cabrera, a basement relief delimited by faults (Figure 1), which bounds the basin to the north (Harvey & Mather, 2015; Giaconia et al., 2012), influenced the formation and closure of the Río Alías Strait.

The geotectonic context in which the ancient straits evolved implied a substantially different evolution of the strait infill. Whereas rift-related dune-bedded successions show a deepening-upward general trend (Reynaud et al., 2013; Longhitano et al., 2014; Longhitano & Chiarella, 2020), the infill of straits evolving in compressional contexts ends with coarse-grained deposits (Martín et al., 2014; Cavazza & Longhitano, 2022).

The purpose of this paper is to describe the deposits filling the Río Alías Strait, detailing their sedimentological characteristics and their spatial and temporal distribution. A depositional model is proposed within the framework of the existing models for similar modern and ancient straits. Finally, the implications of the Río Alías Strait sedimentary record are documented in order to understand the timing and patterns of the uplift and palaeogeographical evolution of the Almería-Níjar Basin and its surrounding basement reliefs. The subject of this study, the deposits of the Río Alías Strait, were partly analysed by Dabrio (1987). In his pioneer work on ancient strait sedimentology, the author only focussed

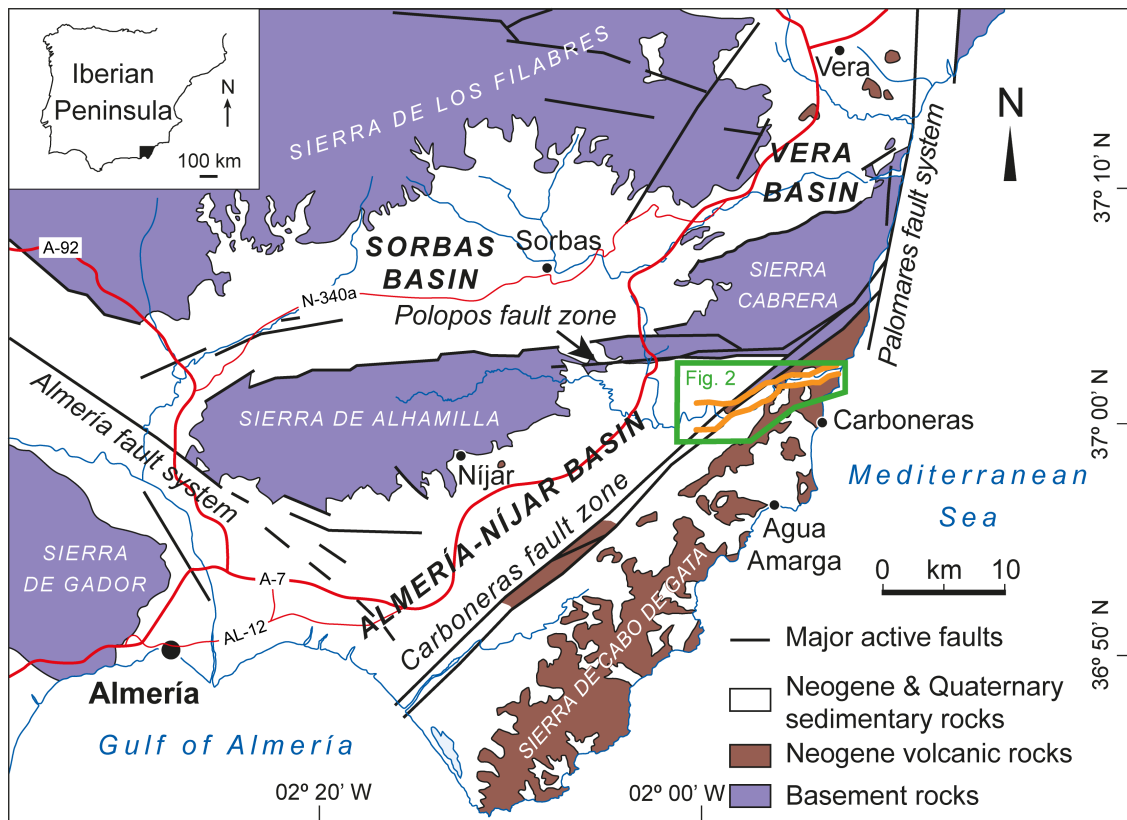


**FIGURE 1** Location of the study area at the north-eastern end of the Neogene Almería-Níjar Basin in the eastern Betic Cordillera in the South-East Iberian Peninsula. Modified after Harvey and Mather (2015). The green polygon shows mapped area in Figure 2. The location of the Río Alías Strait is marked in orange. Red lines correspond to highways (thick lines) and national and regional roads (thin lines).

on the western sector (see below) of the total outcropping area and, after a detailed analysis of the sedimentary structures, concluded that dune migration was controlled by storm-generated currents. Observations of outcrops exposing strait-related deposits and interpretation of facies and structures considering information on strait dynamics generated in the last decades led to a re-interpretation of these deposits as tidally influenced. This new field-based reference case study can be useful for the reconstruction of other straits in the fossil record.

## 2 | MATERIALS AND METHODS

The strait deposits were logged in seven sections at well-exposed outcrops grouped in four sectors forming an ENE–WSW transect: eastern sector (Carboneras N and Loma de la Cañada sections), central-eastern sector (El Llano de Don Antonio and Barranco del Malo sections), central-western sector (La Arboleja section) and western sector (Molino de Arriba and Los Santeros sections). Field-based observations were complemented by petrographic and micropalaeontological analyses of 36 thin sections cut from representative samples. Drone

photogrammetry was used to improve the analysis of depositional architecture and sedimentary structures on vertical cliffs in key study outcrops. The definition of mixed siliciclastic-carbonate sediments (each antithetic component is >10% of the sediment) follows Chiarella and Longhitano (2012). Component proportions were semi-quantitatively estimated and described following an ACFOR scale (abundant  $\geq 30\%$ , common 20–29%, frequent 10–19%, occasional 5–9% and rare <5%). The main lithologies comprising the Río Alías Strait deposits were mapped at a 1:10,000 scale, together with the underlying Miocene rocks.

Aerial photographs of the study outcrops were collected using two ready-to-fly drones helped by a GPS Geomax Series Zenith25 PRO for the acquisition of ground control points: an octocopter Atyges FV8 Topodron carrying a Sony Nex Alpha 7 CMOS 24-megapixel camera and a DJI Phantom 4 Pro, equipped with a DJI CMOS 20-megapixel camera. Three flight paths were conducted at near-parallel viewing angles to capture the three-dimensional (3D) nature of the outcrops. In the first flight, the drone flew along a horizontal axis, with the camera tilted about  $30^\circ$  in the second flight and  $>80^\circ$  in the third flight. Total flight time (without including battery changes) ranged from 20

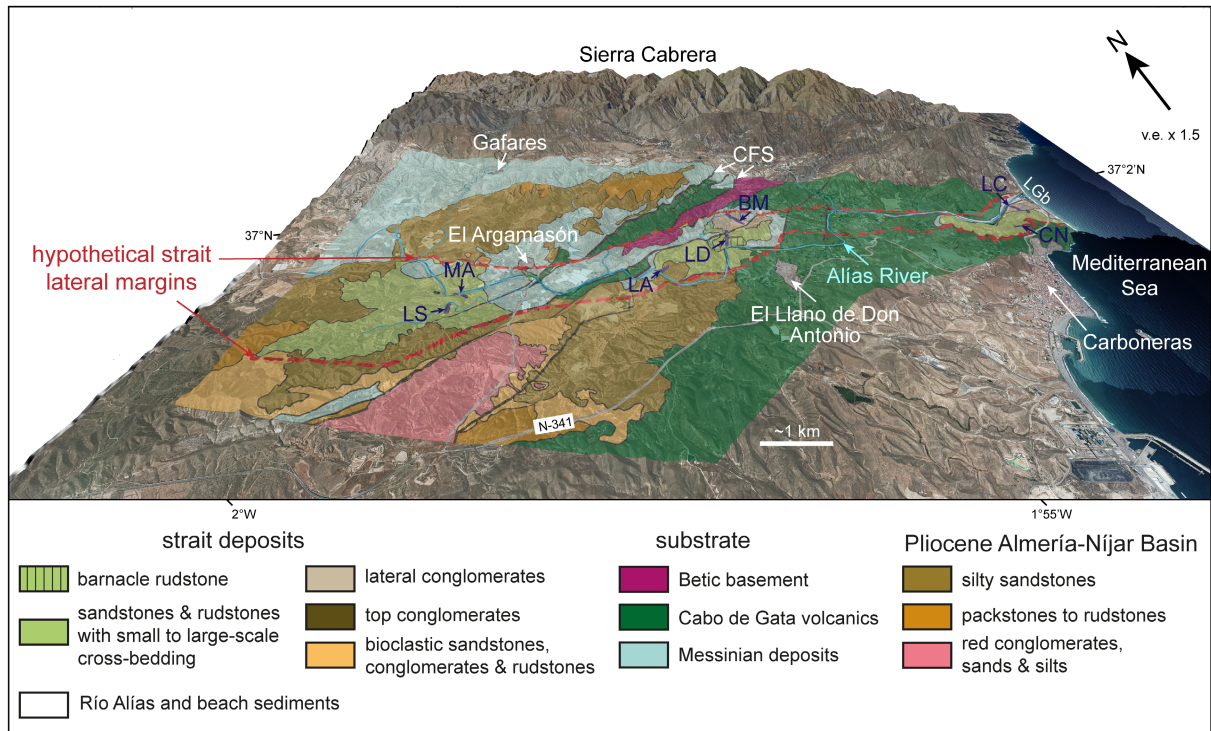


**FIGURE 2** Geological map of the study area with access roads (grey lines) and main villages. BM, Barranco del Malo section; CFZ, Carboneras fault zone; CN, Carboneras N section; LA, La Arboleja section; LC, Loma de la Cañada section; LD, Llano de Don Antonio section; LGb, La Galera beach; LS, Los Santeros section; MA, Molino de Arriba section.

to 35 min at each site. Photographs were taken every 3 s and/or radio-controlled with the drone stationary for specific details allowing for >75% overlap between images. Agisoft Metashape v. 1.8.4 software was used to build the 3D photogrammetric outcrop models. More than 600 photographs with a resolution of 6.29 cm/pixel were processed to generate a dense point cloud (up to 75 million points) and then a triangulated digital surface mesh and overlaying the combined outcrop photomosaic as a surface texture (up to 7.7 million faces). The generated virtual outcrop models were exported in .obj format to the software Virtual Reality Geological Studio v. 3.1 Build 35 (Hodgetts et al., 2007) for geological analysis (geometry, dimensions of the sedimentary bodies and their 3D spatial relationships, measurement of cross-strata orientation, etc.). Bounding surfaces were traced and bedset and foreset thicknesses were measured in the cross-stratified bodies. Grapher 21 software was used to plot rose diagrams and histograms.

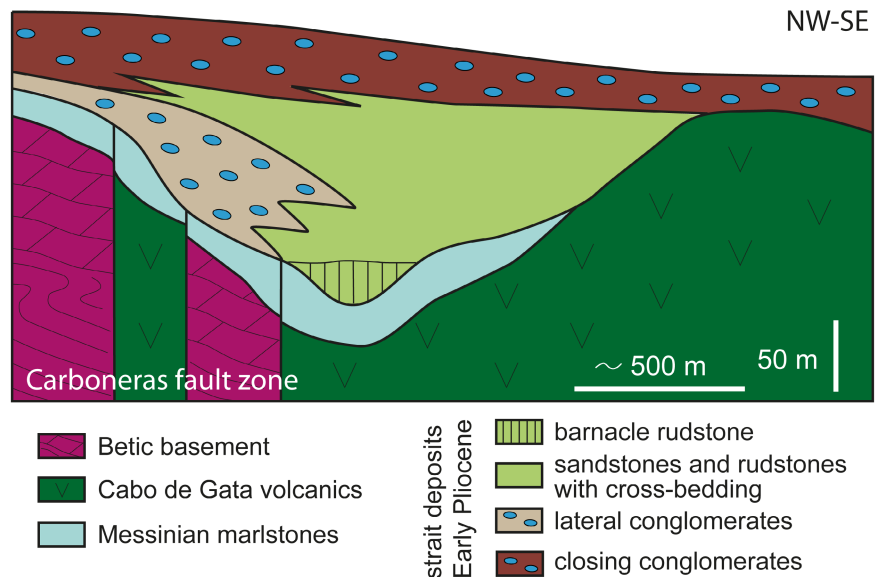
The cross-set thickness and size of the bedforms were classified as thin/small (<40 cm), medium (40–200 cm) and thick/large (>200 cm). This classification was adapted from Ashley (1990) given the importance in tidal settings of submarine dunes >2 m in height for determining the relative predominance of the flood vs ebb currents (Longhitano et al., 2014). The internal organisation of the cross-stratified sets is described according to Anastas

et al. (1997) as simple (cross-sets with conformable strata or laminae) and compound (cross-sets with an internal discontinuity surface).

### 3 | GEOLOGICAL SETTING

The Río Alías Strait was located at the north-eastern end of the Almería-Níjar Basin (Figure 1), which is one of the Neogene intermontane basins that evolved during the structuring and uplift of the Betic Cordillera in southern Spain (Sanz de Galdeano, 1990; Braga et al., 2003; Pedrera et al., 2006; Galindo-Zaldivar et al., 2019). This basin is filled by several sedimentary units separated by unconformities, which accumulated from the middle Miocene onwards (Serrano, 1990; Sola et al., 2017; Galindo-Zaldivar et al., 2019). Miocene units include shallow-water marine carbonates changing laterally to deeper fine-grained deposits, gypsum evaporites and post-evaporitic continental and marine sediments (Dabrio et al., 1981; Fortuin & Krijgsman, 2003; Aguirre & Sánchez-Almazo, 2004). Lower Pliocene marine deposits, including those in the Río Alías Strait, unconformably overlie Tortonian and Messinian units and are overlain by Upper Pliocene and Pleistocene sediments that are extensively exposed. These sediments generally consist of prograding shallow marine and continental materials, whose precise age is poorly

**FIGURE 3** Simplified Miocene to Lower Pliocene stratigraphy at the north-eastern end of the Almería-Níjar Basin.



constrained (Bardají et al., 1997; Aguirre, 1998). The Almería-Níjar Basin is fringed by the Mediterranean Sea at its southern side; is bounded to the north and west by uplifts of the Betic basement; and is delimited to the east-southeast by the outcrops of the Cabo de Gata Neogene volcanic province. The volcanic rocks are partially covered by Neogene sediments accumulated in satellite basins that were connected to the Almería-Níjar Basin at certain phases of their evolution. The boundary between the Cabo de Gata volcanic terrain to the south-east and the Betic basement to the north-west is the CFZ (Figure 1), which runs along the eastern-southeastern half of the Almería-Níjar Basin (Pedrera et al., 2010). The CFZ is a sinistral strike-slip fault system affecting the whole crust (Pedrera et al., 2010). It is one of the shear zones that accommodate the convergence between the African and Iberian plates in the south-eastern Iberian Peninsula since the Late Miocene (Borque et al., 2019). This compressional regime in the Betic Cordillera with a north-west to south-east convergence started in the Tortonian and continued to the Present (Serpelloni et al., 2007; Koulali et al., 2011). The CFZ consists of a series of subvertical fractures that delimit an up to 2 km wide shear zone, which is divided into depressions and topographic highs. In most of its length, the CFZ has an N50E orientation and slightly bends to an N60-65E orientation at its north-eastern extreme. The Río Alías Strait deposits crop out near and in the CFZ (Figures 2 and 3), overlying an erosion surface carved in pre-evaporitic Messinian marls, Messinian gypsum, Cabo de Gata volcanics and Betic basement. The strait deposits change laterally to shallow-water sediments (silty sandstones and packtones to rudstones) of the Almería-Níjar Basin. On the other hand, the northern margin of the basin is delimited by the lateral-oblique Polopos fault zone (Giaconia et al., 2012), a dextral fault system that runs

north of the Río Alías Strait deposits, bounding Sierra de Cabrera, an anticlinal uplift of Betic basement (Figure 1). These two transpressive fault systems influenced the location and evolution of the strait and afterwards affected its infilling deposits. The evolution and final closure of the strait was also controlled by the uplift of Sierra Cabrera.

## 4 | RESULTS

### 4.1 | Facies

Lithology, the nature of biogenic components in the case of carbonates and grain size were used to distinguish 10 major facies (F). Stratal geometries and sedimentary structures allow subfacies to be separated within five of them (Figures 4 through 8).

#### 4.1.1 | F1. Cross-bedded barnacle rudstone

This is a rudstone of granule to pebble-sized, rarely cobble-sized up to 8 cm long, barnacle fragments with rare bivalve bioclasts and occasional to abundant pebble to cobble-sized, up to 20 cm, terrigenous clasts from Messinian marlstone and sandstone, scarce carbonates of the Alpujarride basement, and rare volcanics (Figure 4B). Barnacle clasts are angular to subangular while terrigenous clasts are rounded, some of them bio-eroded. Locally clusters of several barnacle individuals can be observed. These deposits exhibit roughly defined trough cross-bedding (Figure 4A,B) with troughs several metres high and a few tens of metres in length, and foresets pointing mainly to the west. The terrigenous clasts are more abundant at the base of the section.

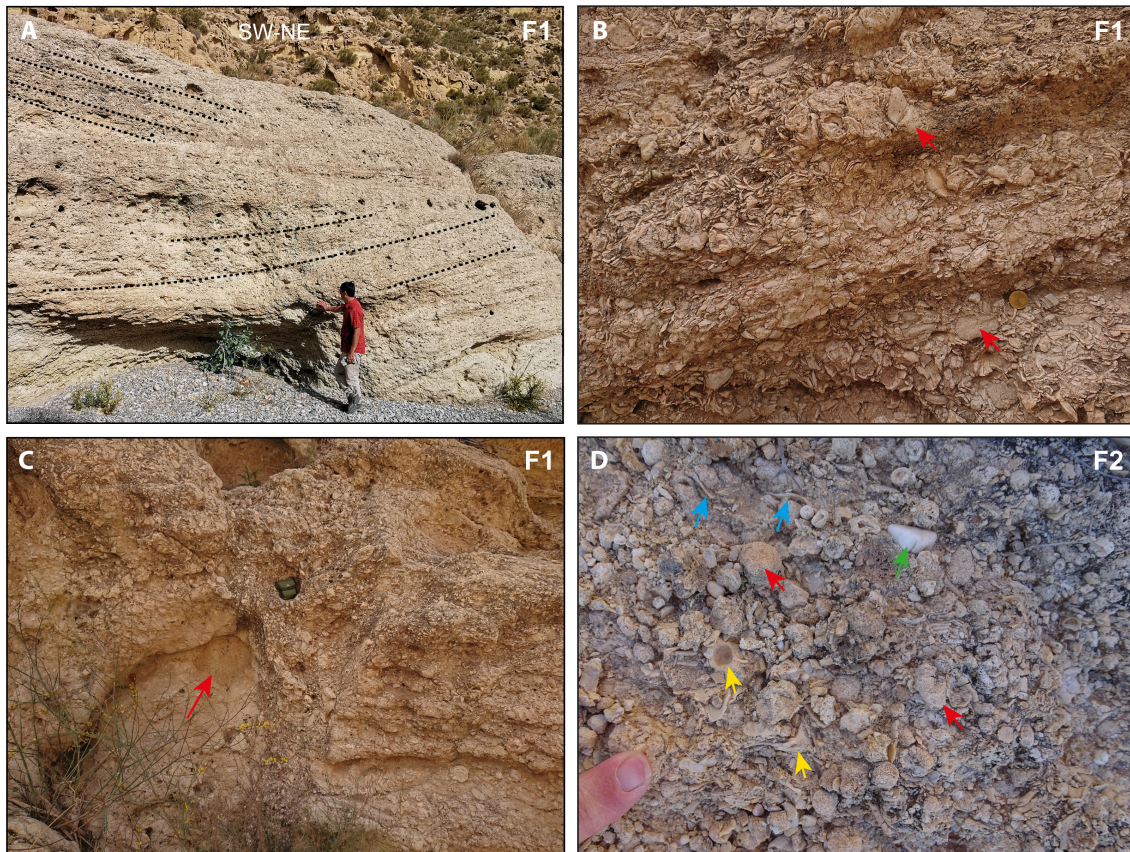


**FIGURE 4** (A–C) Cross-bedded barnacle rudstone facies F1. (A) Roughly defined trough cross-bedding. Person is 185 cm tall. (B) Clasts of Messinian marlstones (red arrows) occur dispersed among barnacle fragments, which are the only bioclasts. Note the rough cross-bedding. Base of El Llano de Don Antonio section. Coin diameter is 23 mm. (C) Neptunian dyke cutting the barnacle rudstone. Two phases of dyke filling can be observed. The first one, mainly consisting of sandstone (arrow) is cut by a second one composed of barnacle rudstone. Base of El Llano de Don Antonio section. Compass case is 8 cm wide. (D) Cross-bedded barnacle/bryozoan/bivalve rudstone facies F2. Fragments of barnacles (yellow arrows), nodular bryozoans (red arrows) and bivalves (blue arrows) are mixed with varying proportions of terrigenous clasts (green arrow). El Llano de Don Antonio section. Maximum finger width is 20 mm.

Centimetre to decimetre-wide neptunian (depositional) dykes cut the cross-beds and are filled by barnacle rudstone, usually finer in size than the rudstone at the dyke walls (Figure 4C), or sandstone rich in bioclasts, mostly planktonic and small benthonic foraminifers and echinoid fragments. The dykes are sealed at their top by overlying cross-bedded rudstone.

#### *Facies interpretation*

Trough cross-bedding suggests accumulation in submarine 3D dunes migrating in a dominant eastward direction. The facies only occur in a narrow belt bounded by Messinian marlstones and volcanic rocks, from which the lithoclasts are derived. Their high degree of roundness, however, indicates reworking by currents, also evidenced by the high degree of fragmentation of balanid skeletons. Barnacles were virtually the only organisms feeding bioclasts. They probably grew attached to the steep strait walls and fell after death to be incorporated into submarine dunes on the strait floor. Balanids obtain

their food by filtering seawater; consequently, areas with strong currents are favourable for their development. The neptunian dykes point to early lithification of the rudstone at the strait floor and the opening of fractures in a locally extensive context. The dykes were filled by sand trapped in them and barnacle bioclasts. This facies is comparable to the coarse-grained gravel pavements that commonly mark the zone of maximum current acceleration in tidal-dominated straits (Longhitano & Chiarella, 2020).

#### 4.1.2 | F2. Cross-bedded barnacle/bryozoan/bivalve rudstone

The barnacle rudstone (F1) gradually changes upwards to a finer-grained rudstone of barnacle fragments with increasing proportions of clasts of bryozoans and bivalves of calcitic shells (oysters and pectinids) and up to 30–35% of terrigenous sand-sized grains and granules to pebbles

of rounded quartz and Messinian marlstone (Figure 4D). Bioclasts are angular to rounded. This rudstone shows poorly defined, large-scale trough cross-bedding pointing to the east and west.

#### *Facies interpretation*

Sedimentary structures suggest an environment of formation similar to that of the barnacle rudstone (F1) although submarine dunes forming this facies were also fed with bioclasts from adjacent shallow-water areas and not exclusively from the barnacles growing on the strait walls. The finer grain size suggests longer transport by dune migration and/or a relative decrease in current energy.

### 4.1.3 | F3. Cross-bedded bryozoan/bivalve packstone to rudstone

This is the most common carbonate lithofacies in the Río Alías Strait deposits. Fragments of bryozoans and calcitic bivalves (oysters and pectinids) are the main components. Echinoid and serpulid clasts are rare to frequent. Coralline algae also rarely occur as fragments and locally as nodules (rhodoliths) concentrated in centimetre-scale layers. Barnacles and small benthonic foraminifers are also rare components. Terrigenous components are always present in varying proportions (frequent to abundant) and transitions from this facies to sandstones (F6) or pebble conglomerates (F9) with bioclasts are common. Two subfacies can be distinguished based on the structures.

F3.1 Large-scale cross-bedded. The deposits exhibit trough and minor planar bidirectional (east–west) cross-bedding up to 11 m in height and tens to a few hundreds of metres in length (Figure 5A). Although bidirectional at facies level, east-oriented and west-oriented cross-beds do not alternate in the study sections but are concentrated in particular intervals. Reactivation surfaces are observed in these large structures and toesets are tangential and occasionally angular. Small-scale planar and trough cross-beds and ripples are superimposed on some larger structures (Figure 5B,C). Foresets in these smaller structures commonly indicate a palaeocurrent direction opposite to their parent structure (Figure 5B,C). Toesets changing from tangential to angular are observed (Figure 5C). Intervals of several decimetres thick plane-bedded sets of this facies occur locally separating large cross-stratified bodies. *Scolicia* bioturbation is widespread. Laminae and beds are defined by different proportions of terrigenous and bioclastic components and grain size (heterolithic rhythms), generally well-sorted and segregated within individual laminae and lacking

mud (Figure 5B,C,D). Bundles of bioclastic and siliciclastic laminae regularly alternate. Alternating thickening and thinning-upward laminasets are also observed, in some cases truncated by major changes in foreset composition (Figure 5B,D).

F3.2 Small to medium-scale cross-bedded. This subfacies show trough cross-bedding decimetres to a few metres thick and metres to few tens of metres wide. Tangential foresets dominate over local planar foresets. Palaeocurrent direction points to east and west, either alternating or showing a preferential orientation within the logged sections. Beds and laminae are defined by changes in bioclast size and terrigenous proportions, which are well segregated. The latter can reach nearly 50% in some beds and merge to sandstones and granule conglomerates within the same bed. *Scolicia* traces are common. This facies commonly alternates in vertical succession with small to medium-scale trough cross-bedded sandstones rich in bioclasts (F6.3).

#### *Facies interpretation*

F3.1 This facies reflects the movement of large-scale subaqueous bedforms under the influence of high-energy bidirectional currents, although with a strong dominance of one transport direction. Its tidal origin is also interpreted by the presence of bundle (heterolithic) cross-lamination, reactivation surfaces and superimposed smaller cross-beds with opposite foreset orientation.

F3.2 These deposits accumulated in subtidal dune fields moved by marine currents. As they alternate in vertical succession with sandstones rich in bioclasts (F6.3), the F3.2 deposits probably formed in periods of more reduced terrigenous input than in those of F6.3.

### 4.1.4 | F4. Flat-bedded packstone to rudstone

Planktonic and benthonic (larger and small) benthonic foraminifers, echinoids, bryozoans and calcitic bivalve fragments are the main components. Rare coralline algae and barnacles also occur. Marlstone and sandstone fragments and quartz and mica grains are common. A muddy matrix is abundant. This facies occurs as decimetre-scale (15–50 cm) beds with flat or slightly erosive, channelised base, massive to roughly laminated, locally with normal grading and commonly alternating with silty facies F5 and massive to flat-laminated sandstones (F6.1).

#### *Facies interpretation*

The alternation with siltstones and the laminar to massive structure suggests that these materials accumulated as low to high-density turbidite deposits in settings not affected by high-energy currents. The abundance of planktonic

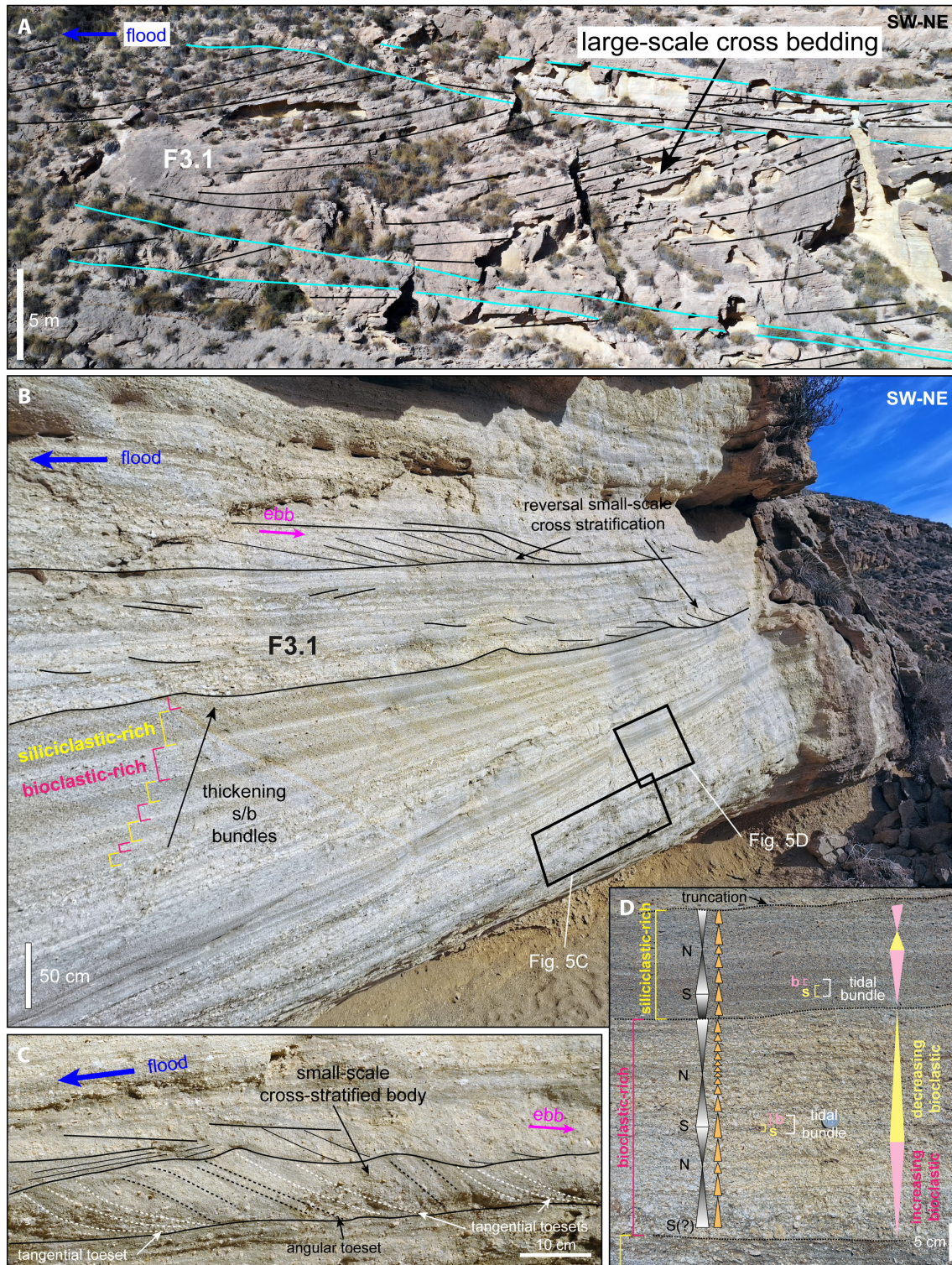


**FIGURE 5** Cross-bedded bryozoan/bivalve packstone to rudstone facies F3.1. El Llano de Don Antonio section. (A) Large-scale cross-bedding. Blue lines are major surfaces separating cross-stratified large-scale bodies (see Figure 8 for location). Note sharp truncation at foreset tops. Palaeocurrent (flood) direction to the SW. (B) The internal structure of large trough cross-beds includes small-scale cross-stratified bodies migrating mainly in opposing direction (ebb) to the main flow (flood). Foresets are defined by changes in grain size, thickness and composition. Note the bundled foreset stratification of alternating beds rich in bioclastic (white) and siliciclastic (dark) components. (C) Close-up view of a small-scale cross-stratified body showing changes in toset morphology from tangential to angular. (D) Close-up view of heterolithic rhythms consisting of bioclastic (b) and siliciclastic (s) laminae and interpreted as tidal bundles (sensu Longhitano et al., 2010; Longhitano, 2011). Thickening-to thinning-upward bundle laminasets that could correspond to spring/neap (S/N) tidal cycles (Longhitano et al., 2012). Also note variations in the thickness of bioclastic and siliciclastic laminae within both bioclastic and siliciclastic-rich beds.

foraminifers indicates a deep-water source for the sediment flows and/or high entrainment of the foraminiferal tests during the passage of gravity flows and erosion of the fine-grained substrate.

#### 4.1.5 | F5. Siltstones and sandy siltstones

Planktonic and small benthonic foraminifers are common in addition to fine-grained terrigenous particles. This facies occurs as two subfacies.

**F5.1** Massive siltstones and sandy silts with blocks The groundmass of fine-grained sediment is structureless except for mottled bioturbation. Highly heterometric angular clasts (up to 80 cm in size) from Messinian marlstone and packstone, which constitute the immediately underlying basement, are either dispersed in the silts or concentrated in channelised bodies decimetres to a few metres in thickness and several metres wide (Figure 6A).

**F5.2** Laminated siltstones and sandy siltstones intercalating packstone to rudstone layers of F4. Bed thickness ranges between 5 cm and 80 cm. Lamination is parallel to bedding and defined by changes in grain size and the proportion of bioclasts (Figure 6A). Bioturbation is common. Some layers are packstone to rudstone mainly composed of planktonic foraminifers. Benthonic foraminifers, echinoid, bivalve and bryozoan fragments are secondary bioclastic components. Bioclastic layers often exhibit erosive bases. Marlstone fragments, quartz and micas appear in varying proportions (up to 30–40%).

##### *Facies interpretation*

These deposits accumulated in relatively deep-water settings unaffected by high-energy currents. In F5.1 clasts

from the adjacent basement fell into the setting either isolated and dispersed or in confined flows generated by mass-transport processes. The laminated F5.2 deposits probably formed as low-density sediment gravity flows. Massive F5.1 deposits probably represent the same type of deposits as F5.2 but the original lamination could be obliterated by bioturbation.

#### 4.1.6 | F6. Medium to coarse sandstone

These deposits are mainly composed of rounded to sub-rounded grains of quartz and quartzite, with secondary mica, feldspar, carbonate and opaque minerals. They contain varying bioclastic proportions and transitions from sandstone rich in bioclasts to packstone and rudstone rich in terrigenous grains (facies F3 and F4) are common at the centimetre to decimetre-scale. Bedding and lamination are marked by changes in grain size, nature of terrigenous grains and bioclastic proportion. Four subfacies can be distinguished according to the type and scale of the structures.

**F6.1** Massive to flat-laminated. Lamination is defined by changes in the proportion of bioclasts and grain size. Mottled and escape bioturbation is common (Figure 4F). Laminated beds are up to 40 cm thick and no bedding is observed in massive intervals of this facies, which can be up to 12 m thick. Small ripples (<4 cm thick) locally occur. This facies commonly alternates with laminated beds of F4.

**F6.2** Large-scale trough cross-bedded. These sandstones exhibit large-scale trough cross-bedding up to 5 m in thickness and up to 40 m in length (Figure 7A,B). Toesets are mainly tangential and locally angular (Figure 7A) and

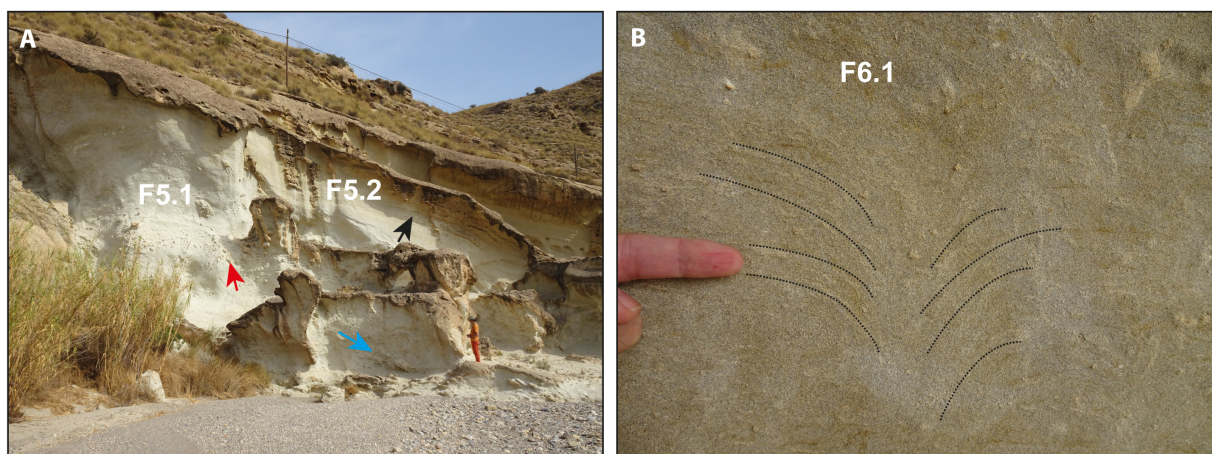


**FIGURE 6** (A) The base of La Arboleja section consists of massive siltstones and sandy siltstones with blocks (F5.1). The marlstone blocks from the Messinian basement occur either dispersed in the siltstone (red arrow) or concentrated in channelised bodies (blue arrow). Massive siltstones change upward to laminated siltstones (F5.2) (black arrow). Person is 190 cm tall. (B) Escape bioturbation in flat laminated medium sandstones (F6.1). La Arboleja section. Maximum finger width is 22 mm.

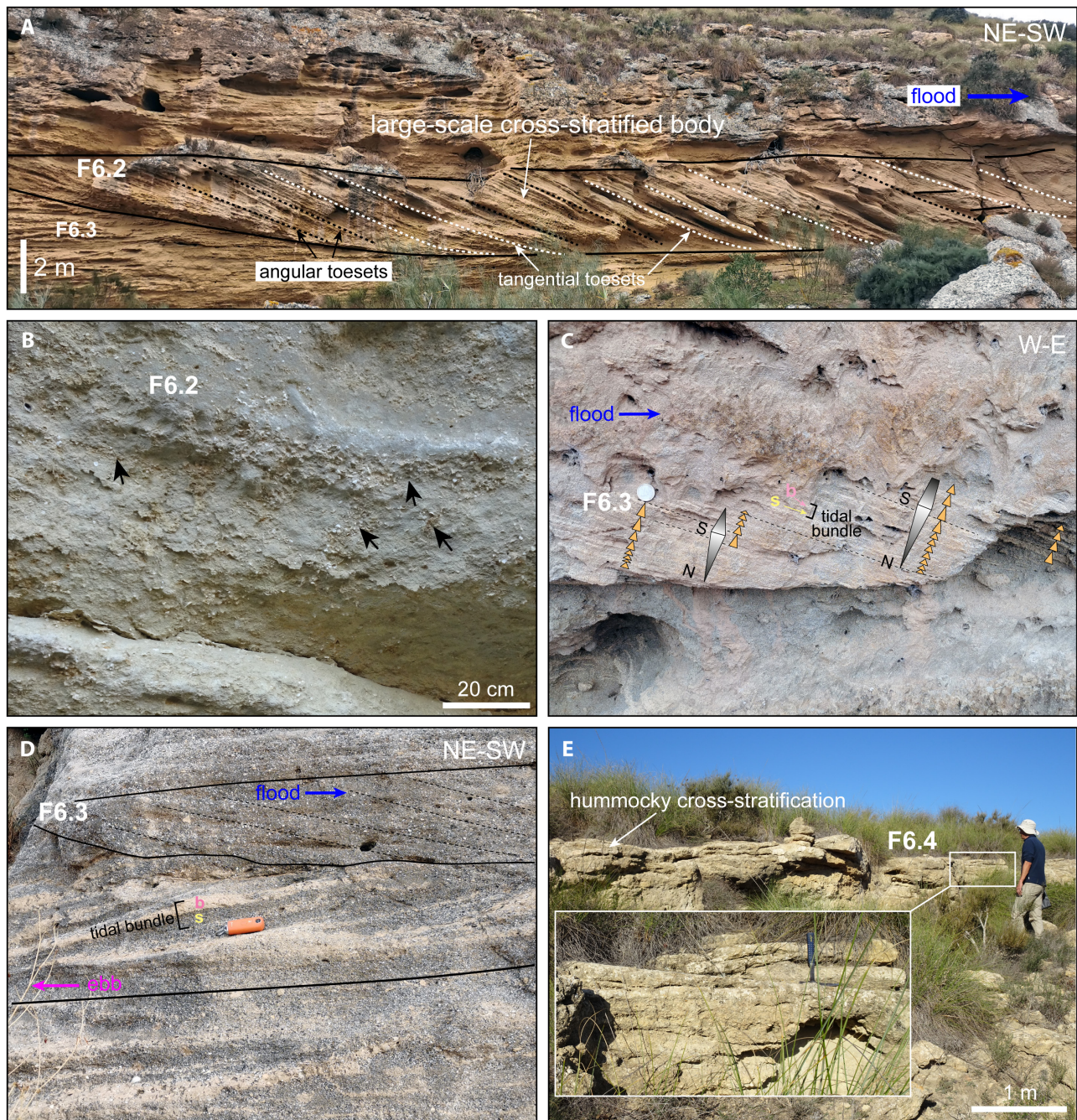


**FIGURE 7** (A, B) Large-scale trough cross-bedded sandstones F6.2. Molino de Arriba section. (A) Large-scale cross-stratified body exhibiting tangential to angular toesets. Palaeocurrent direction is to the West. (B) Bioclasts occur in varying proportions and concentrate at the base of troughs (black arrows) and in burrows (red arrows). (C) Close-up view of medium-scale cross-bedded sandstone F6.3 showing bundle heterolithic stratification formed by alternating bioclastic (b) and siliciclastic (s) laminae. Thickening to thinning-upward laminasets suggest spring/neap (S/N) tidal cycles (Longhitano, 2011; Longhitano et al., 2012). Molino de Arriba section. Coin is 2.3 cm in diameter. (D) Small-scale cross-bedded sandstone F6.3 exhibiting bidirectional foreset migration. Packstone to rudstone laminae can be locally abundant forming heterolithic bioclastic-siliciclastic (b-s) lamination that can be interpreted as tidal bundles (Longhitano, 2011; Longhitano et al., 2012). Loma de la Cañada section. Keys are 8 cm in length. (E) Hummocky cross-bedded sandstones F6.4. Zoomed inset shows rough lamination. Molino de Arriba section. Hammer is 33 cm long.

their migration direction is bidirectional towards the east and west.

F6.3 Small to medium-scale trough cross-bedded. Metre-scale bidirectional (east–west) trough

cross-bedding (locally planar) is pervasive (Figure 7C). Foresets in these structures have tangential and angular toesets, sometimes with changes between them in the same cross-bedded body. Laminae are frequently

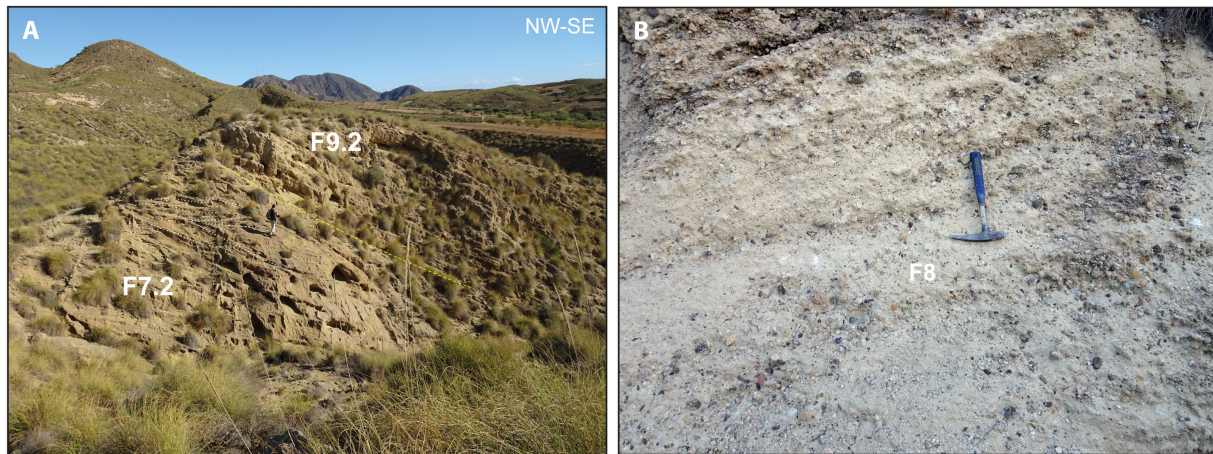


**FIGURE 8** (A) Medium-scale trough cross-bedded granule conglomerates F7.2 underlying clino-bedded pebbly conglomerates F9.2 that prograde southward. Barranco del Malo section. Person is 185 cm tall. (B) Matrix-supported pebbly conglomerate F8 rich in bioclasts. Note rough cross-bedding in the upper half of the picture. Base of Barranco del Malo section. Hammer is 33 cm long.

defined by different and well-segregated proportions of bioclastic and terrigenous components forming a regular bundle (heterolithic) lamination (Figure 7C,D). Alternating thicker and thinner foreset laminae are also observed (Figure 7C). Laminae and beds of rudstone, with concentrations of bivalve and bryozoan bioclasts are occasional to common. Rudstone beds usually show irregular bases and normal grading. Bioclasts can also be concentrated in bioturbation traces. Packages, several metres in thickness, dominated by either medium or coarse sand alternate throughout the succession. This facies also alternates with F3.2.

F6.4 Hummocky cross-bedded. Coarse sandstones with granules, small pebbles and large bioclasts with an erosional base and exhibiting simple, isotropic hummocky cross-bedding (Figure 7E). Individual beds are 10–25 cm thick and are roughly laminated (Figure 7E), with dipping angles of  $<15^\circ$ . This facies occurs only locally intercalated within trough cross-bedded sandstones (F6.2).

#### *Facies interpretation*

F6.1 The occurrence of this laminated facies alternating with F4 suggests a similar origin as turbidity flows accumulated in areas not significantly affected by currents. The relative proportions of bioclasts in the flow source marked the transition from F6.1 to F4. Massive intervals of this facies are interpreted as turbidite flows of higher density than those of laminated deposits.

F6.2 Sedimentary structures are similar to those in F3.1 packstones and rudstones and suggest a similar origin, that is, large dunes moved by high-energy currents, although in a relatively more siliciclastic setting. A tidal origin is interpreted based on the palaeocurrent migration reversal and heterolithic bundles.

F6.3 This subfacies formed in subtidal dune fields fed by mixtures of terrigenous particles from the surrounding highs and varying amounts of bioclasts produced on the dune fields or in adjacent shallow-water areas being hydraulically mixed.

F6.4 Hummocky cross stratification is indicative of short-term periods of storm waves temporarily influencing or reworking the top of the dune fields, thus indicating a relative depth close to the storm wave base level. Concentration of larger lithoclasts and bioclasts on an erosive basal surface is also characteristic of storm deposits.

#### 4.1.7 | F7. Granule conglomerate

This is a clast-supported conglomerate of granules of quartz and quartzite within a sand matrix. Two subfacies can be separated according to the scale of the structures.

F7.1 comprises granule conglomerates with large-scale cross-bedding pointing to the west. Rounded fragments of bryozoans, coralline algae, echinoids, bivalves and marlstone are rare to common.

F7.2 consists of granule conglomerates with bidirectional (east-dominated) small to medium-scale cross-bedding (Figure 8A). Rare to common bioclasts of bivalves (oysters and pectinids) and balanids occur among the terrigenous clasts. They also appear concentrated in thin beds (a few decimetres thick) with erosional bases and normal grading.

#### *Facies interpretation*

F7.1 Large-scale dunes transported coarse-grained sediment under the action of high-energy currents. Their occurrence intercalated between carbonate-dominated facies F3 (see Section 4.2) points to a higher sediment input

to the strait axis or reduced carbonate production in local factories.

F7.2 The clasts fed from the basement highs by fan deltas were reworked and incorporated in submarine dunes together with varying proportions of bioclasts. Beds of shell concentrations could result either from high-density currents entering the shallow-water strait or from storm events (Schmidt & Seyfried, 1991; Bressan et al., 2013).

#### 4.1.8 | F8. Matrix-supported pebbly conglomerate rich in bioclasts

This facies consists of poorly sorted granules to pebbles (and rare cobbles up to 10 cm in size) in a matrix that varies from packstone to sandstone with a muddy matrix even at the thin section scale, depending on the relative proportion of bioclasts and terrigenous grains, which are poorly segregated (Figure 8B). The clasts can be dispersed in the matrix or concentrated in poorly defined lenses several centimetres thick and some decimetres wide. Bioclasts is derived mainly from bivalves, barnacles, echinoids and planktonic and benthonic (larger and small) foraminifers. These deposits show a rough small to medium-scale cross-bedding marked by clast lenses (Figure 8B).

##### *Facies interpretation*

This facies is interpreted to be the result of fluvial sheet flows or hyperconcentrated flows entering a shallow-marine area in a fan delta setting at the toe of the antecedent relief of Sierra Cabrera. The clasts provided by the initial phases of the fan delta mixed with bioclasts during their emplacement and were later reworked in a subtidal setting. Poorly developed cross-bedding and coarse-grained matrix content suggest a position at the strait margin where the tidal current strength was dissipated by friction.

#### 4.1.9 | F9. Pebbly conglomerate

This facies comprises a clast to matrix-supported conglomerate of rounded to subrounded granules to pebbles in a sandstone matrix. Minor cobbles up to 10 cm and coarse sandstone intervals can locally occur. Most terrigenous clasts are quartzite with secondary dolostones and schists from the Betic basement in Sierra Cabrera. Pebble to cobble-sized bioclasts are rare to common, locally concentrated in thin (<10 cm) lenses. They are mainly fragments of bivalves, bryozoans, barnacles, echinoids, coralline algae and benthonic foraminifers. The matrix is similar to the coarse sandstone lithofacies F6.

Two subfacies can be distinguished:

F9.1 Small to medium-scale trough cross-bedded. The matrix can locally be a rudstone similar to facies F3. Shell concentrations occur as decimetre-scale lenses with irregular bases and rough normal grading.

F9.2 Clino bedded. They occur in foresets that dip 10–15° generally southwards (Figure 8A), becoming nearly horizontal (topset) upslope. Beds are generally thin, centimetres to a few decimetres thick, with planar or slightly erosive bases and parallel lamination in the finer-grained lithologies. Ripples migrating to the west can locally be observed. Some intervals show decimetre-thick, amalgamated channelised beds, which include the coarsest and heterometric clasts up to cobble size. Bioclasts occur dispersed among the terrigenous clasts or concentrated in beds with erosional bases, a few decimetres thick and few metres in lateral extent.

##### *Facies interpretation*

These conglomerates were deposited in small coarse-grained deltas at different locations at the toe of the antecedent relief of Sierra Cabrera to the north.

F9.1 The trough cross-bedding indicates reworking of the pebbly conglomerates incorporated in submarine dunes. Terrigenous grains mixed with abundant biogenic particles produced by invertebrates and coralline algae in the delta front and adjacent shallow areas.

F9.2 The clinobeds represent the delta foresets relatively unaffected by marine currents. They reflect either a marginal strait location (lateral conglomerates in Figures 2 and 3), lower current strength able to mobilise coarse-grained sediments and/or strait closure (closing conglomerates in Figures 2 and 3).

In both subfacies, shell beds probably accumulated during storm or sheet-flood events.

#### 4.1.10 | F10. Breccia of volcanic pebbles to boulders in a sandy matrix

This is a poorly sorted clast-supported breccia of angular clasts from the immediately underlying volcanic basement. This facies forms wedge-shaped deposits up to 3 m thick that pinch out against the substrate. The matrix among the clasts is a sandstone with abraded bioclasts of bivalves, bryozoans and minor coralline algae.

##### *Facies interpretation*

The angularity of the clasts, their clast-supported texture and their lithological affinity with the underlying basement rocks and the wedge shape suggest accumulation at a rocky shore of clasts fallen from the emergent underlying basement (Semeniuk & Johnson, 1985; Gupta & Allen 1999; Sola et al., 2022), as the shoreline

retreated with a relative sea-level rise reflected by the onlapping of Pliocene sediments on the Cabo de Gata volcanics at the southern margin of the Río Alías Strait. Accumulation in subtidal settings is evidenced by invertebrate and coralline algal bioclasts mixed with the volcanic clasts.

## 4.2 | Outcrop localities

### 4.2.1 | Eastern sector

In this sector, the Lower Pliocene deposits related to the Río Alías Strait unconformably overlie Messinian marlstones and breccias at the north-western side of the outcrop and onlap volcanic rocks to the south (Figure 3). The fine-grained deposits cropping out close to the shoreline (La Galera beach; Figure 2) contain planktonic foraminifers indicative of an Early Pliocene age (Aguirre, 1998).

#### *Loma de la Cañada section*

The base of the section is located at the southern slope of the Alías river valley at 600m from the La Galera beach (Figure 2). The lower 10.5m strait deposits at this section consist of thick bedsets of simple, east-west oriented trough cross-bedded conglomerates (F9.1) with common pebble-sized bioclasts including pectinids, oysters, bryozoans and rhodoliths (Figure 9A). The clasts are made of quartzites and secondary dolostones evidencing their provenance from the antecedent upland of Sierra Cabrera to the north. The matrix is coarse sandstone to rudstone due to varying proportions of terrigenous grains/bioclasts. The overlying 105m comprise alternating bed packages of pebbly conglomerates (F9.1), granule conglomerates (F7.2) and medium to coarse sandstone (F6.2), all of them with varying proportions of bioclasts, usually concentrated in laminae and beds. These deposits exhibit decimetre to metre-scale simple, mainly east-oriented trough cross-bedding except for the medium sandstones, probably due to their poor exposure. Grains are mainly of quartzite from the Betic basement in Sierra Cabrera. The upper 25m include cross-bedded rudstones (F3.2) with common to abundant quartzite pebbles and simple cross-bedded medium packstones (F3.2). Bioclasts in F3.2 are mainly pectinid and oyster fragments, with secondary bryozoans and coralline algae.

*Carboneras N section.* The base of the section is located at the northern edge of Carboneras by the road to Mojácar (Figure 2). The base of the Pliocene deposits is a breccia of volcanic pebbles to boulders in a siliciclastic sandy matrix with bioclasts (F10) (Figure 9B). The breccia varies

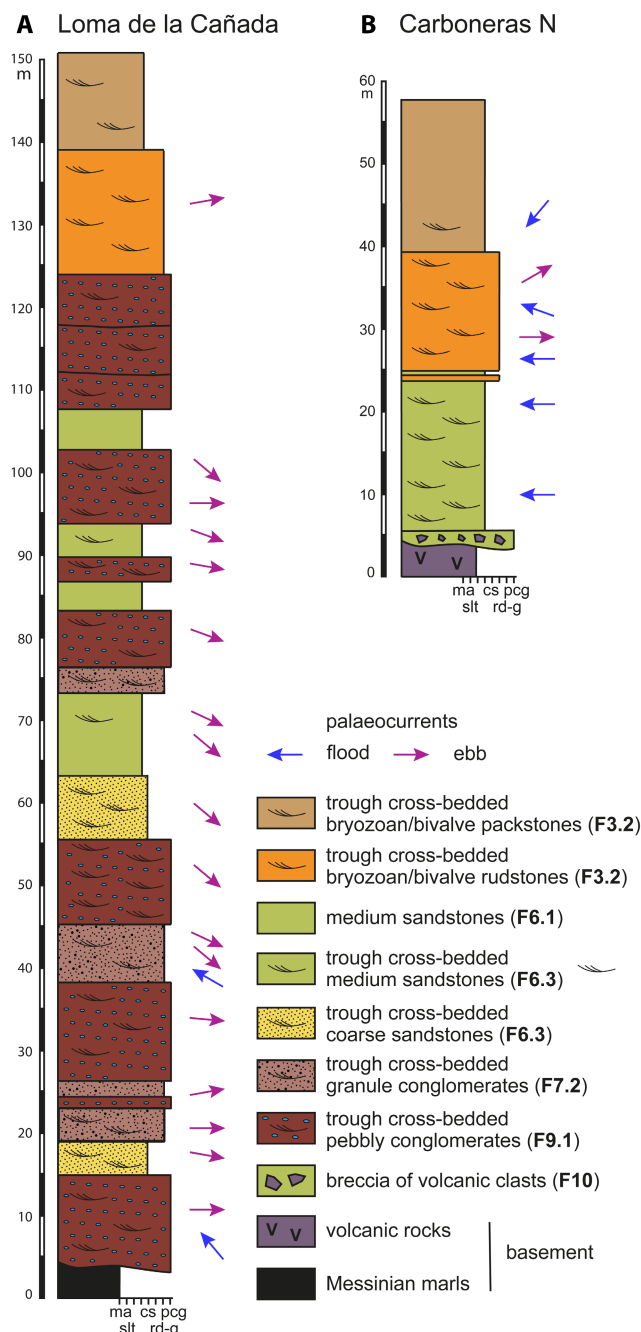


**FIGURE 9** Stratigraphic columns of the Loma de la Cañada (A) and Carboneras N (B) sections in the eastern sector. Grain-size scale: Ma = marl; slt = silt; cs = coarse sand; rd-g = rudstone-granule conglomerate; pcg = pebbly conglomerate.

from decimetres to a few metres in thickness filling an irregular surface on top of the volcanic basement, which locally includes a different breccia, the “brèche rouge of Carboneras” (Montenat et al., 2000; Krautworst & Brachert, 2003). Similar breccias overlying the Cabo de Gata volcanics range in age from Late Miocene to Early Pliocene in localities in which their age can be constrained either by radiometric ages of underlying volcanics or by biostratigraphic ages of overlying fine-grained sediments

(Serrano, 1992; Brachert et al., 2002; Martín et al., 2003). At the Carboneras section, the breccia at the base (F10) is overlain by medium sandstones (F6.3) that change laterally (eastward) to finer-grained silts (F5.1) dated as Early Pliocene by planktonic foraminifers (Aguirre, 1998). These medium sandstones are arranged in a 19 m thick stratal package and show a varying bioclastic content, close to 40% in some beds. Bioclasts range from sand grade to pebble in size and can locally be concentrated in thin lenses. Beds are centimetres to decimetres thick and exhibit small to medium-scale (planar) trough cross-bedding pointing mainly towards the east. *Scolicia* traces are common on bed surfaces. The sandstones pass gradually upwards to a 15 m thick rudstone interval (F3.2) with rare to common sand-sized terrigenous grains. Bioclasts are mostly bivalve fragments (pectinids and oysters) and secondary bryozoans and barnacles. The rudstones show a poorly defined, small to medium-scale, bidirectional (east-west) simple trough cross-bedding. They find up to a 18 m thick packstone strata (F3.2) with small to medium-scale simple trough cross-bedding in the lower part pointing towards the south-west, although no structures can be observed in the top 15 m due to vegetation cover.

**Architecture and palaeocurrents.** The cross-stratified strait deposits in the eastern sector form a coarse-grained siliciclastic and mixed siliciclastic-carbonate succession between 55 m and 145 m thick that resulted from the vertical accretion of small to medium-scale, simple, mostly 3D dunes with tangential foresets. Sediments in the Loma de la Cañada section were fed by a small fan delta sourced from Sierra Cabrera. Palaeocurrents obtained from cross-bedded foresets and trough axes indicate an asymmetrical (east-dominated) bidirectional migration of submarine dunes. These features are consistent with the accumulation of the Lower Pliocene deposits at the eastern sector in a dune-bedded strait zone sensu Longhitano (2013).

#### 4.2.2 | Central-east sector

##### *El Llano de Don Antonio section*

The section is located west of the El Llano de Don Antonio village, on the northern side of the Alías river valley (Figure 2). The basal Pliocene deposits unconformably overlie Messinian marlstone with intercalated diatomitic marlstone and turbiditic packstone beds. The Pliocene succession here is up to 135 m thick. The logged stratigraphic column, about 90 m in thickness, begins with a 10 m thick, trough cross-bedded barnacle rudstone (F1) (Figure 10A). Pebble to cobble clasts from the basement are concentrated in the lowest metres. The bioclast size

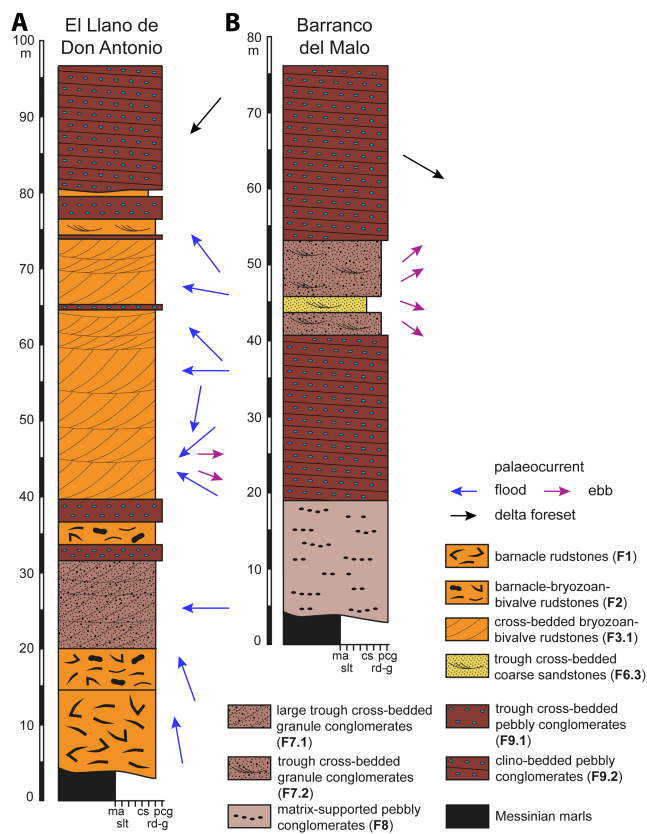


**FIGURE 10** Stratigraphic columns of sections in the central-eastern sector. Grain-size scale: Ma, marl; silt, silt; cs, coarse sand; rd-g, rudstone-granule conglomerate; pcg, pebbly conglomerate.

decreases in the following 4.5 m composed of barnacle-bryozoan-bivalve rudstone (F2). After a 12 m thick interval of granule conglomerate with frequent bioclasts (F7.1), the succession is dominated by rudstone (F3.1) with varying proportions (rare to abundant) of terrigenous grains, mainly quartz and quartzite. Thinner bodies, up to 3 m thick, of pebbly conglomerates intercalate in the rudstone (F9.1). All these deposits exhibit large-scale cross-bedding indicating an east-dominated palaeocurrent direction. Overlying an erosion surface, the topmost 18 m of the succession comprise pebbly conglomerates arranged in clinobeds (F9.2) dipping 10–15° southward.

##### *Barranco del Malo section*

The base of this section is located about 400 m north-northwest from the El Llano de Don Antonio Section (Figure 2). The ca 70 m thick Lower Pliocene deposits unconformably overlie Messinian marlstones intercalating turbiditic packstones (Figure 10B). The base of the Pliocene succession consists of a matrix-supported pebbly conglomerate rich in bioclasts (F8), up to 14.5 m in thickness. Terrigenous clasts are mostly of Messinian marlstone, volcanics and dolostone, limestone and quartzite from the Betic basement. Carbonate clasts are bioeroded by *Entobia*

(sponge borings). These deposits are overlain by pebbly conglomerates (F9.2) with clasts mostly of quartzite and secondary dolostones, and micaschists. Lenses of bioclast concentrations are dispersed at different levels. The conglomerates change upwards into a 12 m thick interval of granule conglomerates (F7.2) intercalating coarse to very coarse sandstones (F6.2), both showing small to medium-scale, east-oriented trough cross-bedding and beds of shell concentrations. Clusters of the oyster *Neopycnodonte* occur as lenses in the sandstones. The upper part of the section comprises up to 25 m of pebbly conglomerates arranged in clinobeds (F9.2) with slightly erosive bases prograding southwards. As in the underlying units, grains in these conglomerates are mainly of quartzite from the Betic basement in Sierra Cabrera.

### Architecture and palaeocurrents

The very well-exposed succession of carbonates and lesser siliciclastics in the Llano de Don Antonio is organised in trough (locally planar) cross-stratified bodies up to 14.5 m thick (Figure 11). The internal architecture of these bodies includes simple (2–10.5 m thick) and compound (3.3–14.5 m thick) cross-bedded foresets dipping 10–25° (commonly between 15° and 20°). The basal surface of dune migration extends a few hundreds of metres over a slightly concave-up discontinuity (Figure 11)

that sharply erodes the underlying foresets (Figures 5A and 11A). The orientation of the surfaces bounding cross-stratified bodies can be different from the overlying foresets. Compound dunes comprise 2–3 bedsets and the height of the foresets between reactivation surfaces is between 50 cm and 11.2 m. The reactivation surfaces are plane to slightly concave and are oriented at 20–50° with respect to the orientation of foresets. In some cases, major reactivation surfaces between dune bedsets are overlain by plane-bedded deposits <1 m thick locally changing laterally to small to medium-scale dunes (Figure 12B). The smaller bedforms in compound dunes migrate in the same direction as their larger parent structures. The dominant migration of both simple and compound dunes ranges between east-southeast and north-northwest with a radial distribution either along the downcurrent direction or the full outcrop locality (Figure 11A). Slightly opposite palaeocurrents to the north north-northeast are subordinated and those with a clear east component in the large cross-bedded bodies are located at the base of the section (facies F1 and F2; Figure 10A). Only small dunes (<40 cm thick cross-beds) superimposed onto larger structures exhibit a clear bidirectional orientation pattern (Figures 5B,C and 12C).

Although it may change laterally in the migration direction, large F1–F2 cross-stratified bodies change

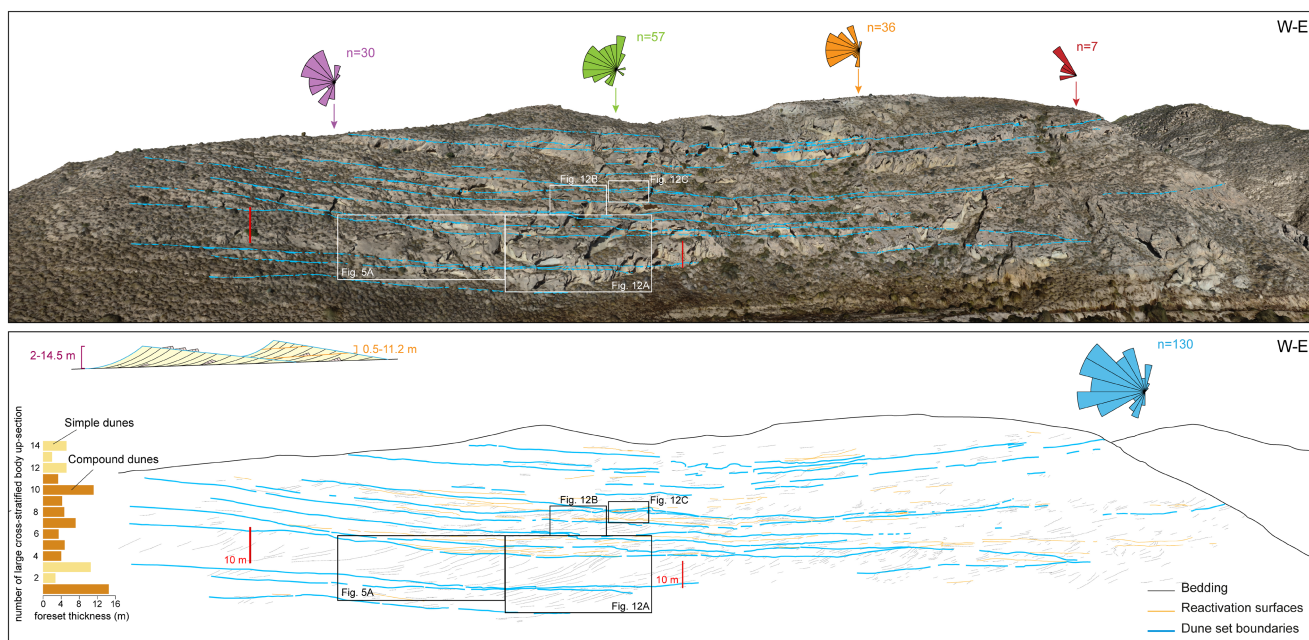


**FIGURE 11** Northward-oriented virtual outcrop model of El Llano de Don Antonio section in the central-eastern sector showing large cross-stratified bodies (set bounding surfaces in blue) that include simple and compound dune foresets (reactivation surfaces in orange). Histogram shows the foreset height variation of the large bedforms up-section. Palaeocurrent diagrams along an E–W transect (roughly the orientation of the Río Alías Strait) (over the 3D model) and for the full section (in blue in the interpreted model). Note the radial distribution of the palaeocurrents with a dominant westward direction and minor opposite direction. Here, the Río Alías Strait formed a lobate body or constriction-related delta (*sensu* Dalrymple, 2023) accumulated in a dune-bedded zone (see Section 5 for details).

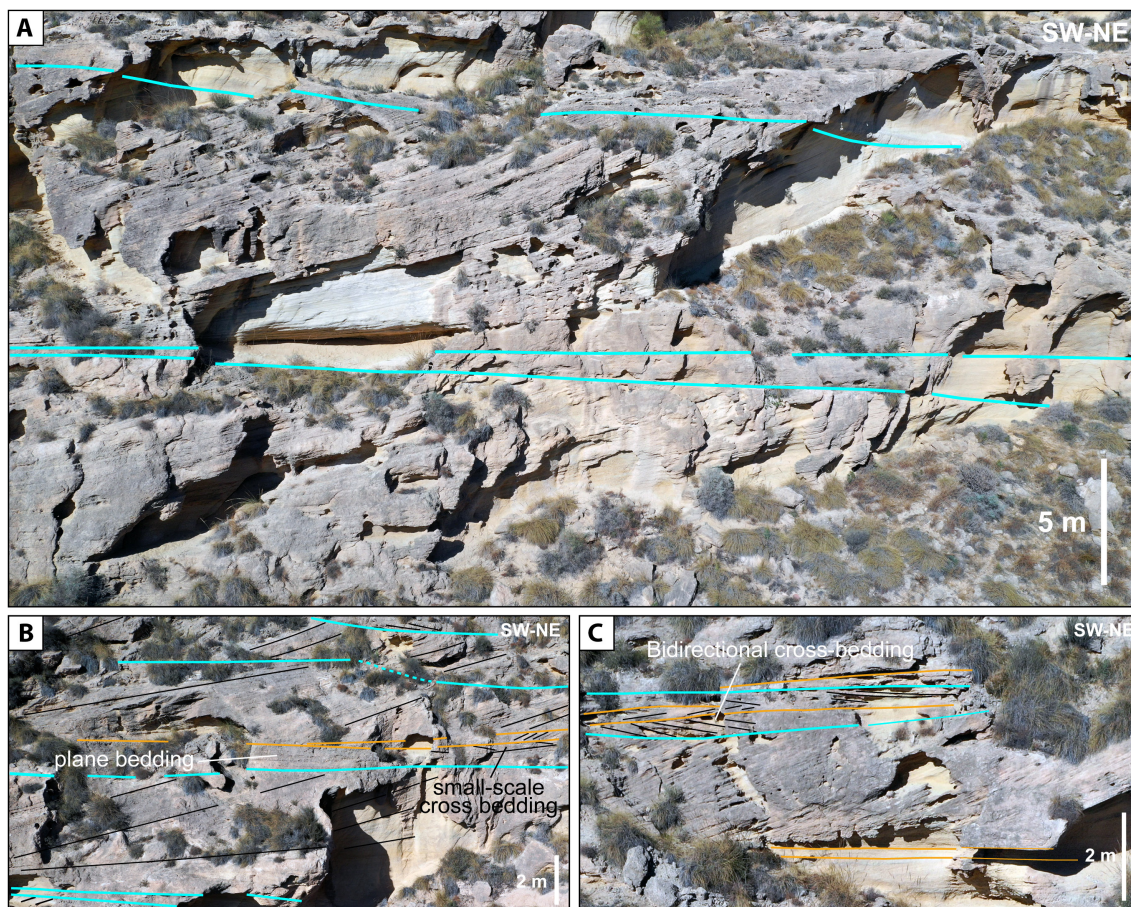


**FIGURE 12** Outcrop view of strait deposits in the El Llano de Don Antonio section (see location in [Figure 11](#); line colour code as in [Figure 11](#)). (A) Large simple dunes migrating westward. Note the sharp erosive contact between the cross-bedded bodies (bounding surfaces in blue). (B) Close-up outcrop view of large dune sets separated by a plane-bedded interval including small-scale cross-beds. (C) Close-up outcrop view of a medium-scale compound dune (between dune bounding surfaces in blue) on top of a larger one showing small-scale bidirectional (herringbone) stratification.

vertically to large-scale simple dunes that are replaced by smaller compound dunes ([Figure 12](#)). These dunes seem to increase in size up-section, although the poorer lateral preservation of bounding surfaces in the upper part of the outcrop prevents confirmation of such size variation.

The S-dipping, coarse-grained, dominantly clino-bedded conglomerates at the Barranco del Malo section prograde over terrigenous-dominated, smaller-scale cross-stratified bodies (up to 2.5 m) than in the Llano de Don Antonio section. Palaeocurrents obtained from cross-bedded foresets in these smaller structures indicate that the dominant migration of the bedforms is to the east.

The accumulation of cross-bedded deposits several tens of metres thick in the Llano de Don Antonio points to a highly depositional zone consistent with a dune-bedded strait zone (*sensu* Longhitano, 2013). The oblique sediment supply from a coarse-grained delta is indicative of a strait-margin zone (Rossi et al., 2017; Chiarella et al., 2020; Longhitano & Chiarella, 2020).

#### 4.2.3 | Central-west sector

##### *La Arboleja section*

This section is located at a dogleg of the Alías River, 700 m north-west of the remains of La Arboleja ([Figure 2](#)), an old country house. Pliocene sediments unconformably overlie Messinian marlstones intercalating turbiditic packstone beds. The lowest Pliocene deposits consist of siltstones (F5.1), 9 m thick, including debris (up to boulders in size) from the Messinian basement, either dispersed or concentrated in channels ([Figure 13](#)). The grain size in the overlying succession, 30 m in thickness, increases upwards from flat-laminated siltstones to siltstones (F5.2) intercalating thin flat-bedded packstones to rudstones (F4) overlain by medium sandstones (F6.1), which in the upper 15 m, also intercalate flat-bedded packstones to rudstones (F4). Sandstones locally show small ripples. These deposits are overlain by flat-bedded rudstones (F4; 14 m) locally with slightly erosive bases, followed by cross-bedded medium sandstones (F6.3; 3 m). The upper part of the section

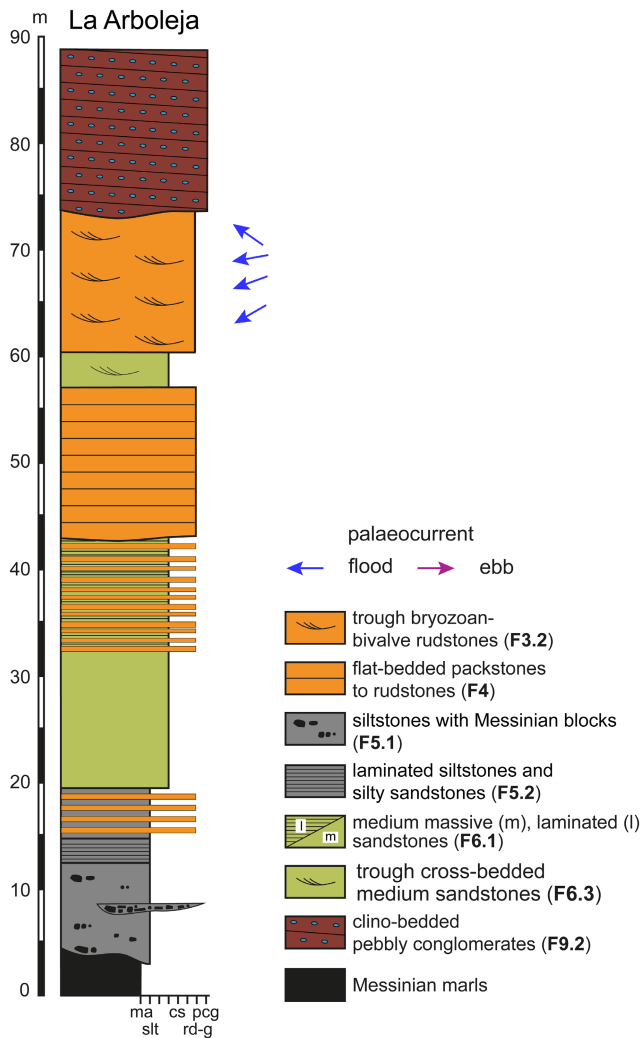


**FIGURE 13** Stratigraphic column of section in the central sector. Grain-size scale: cs, coarse sand; Ma, marl; pcg, pebbly conglomerate; rd-g, rudstone-granule conglomerate; slt, silt.

comprises small to medium-scale cross-bedded rudstones (F3.2), 13.5 m in thickness, with a westward-dominated palaeocurrent direction, and pebbly conglomerates (15 m) arranged in clinofolds (F9.2) dipping southwards.

#### *Architecture and palaeocurrents*

The first ca 75 m of the mixed siliciclastic-carbonate strait succession in the central-west sector records an upward coarsening and carbonate increase capped by very coarse-grained deltaic deposits. Mass-transport deposits and thin-bedded turbiditic deposits are replaced by bedsets of simple cross-stratified bodies that exhibit bidirectional (westward-dominated) foreset migration. This internal architecture is indicative of a gradual change in current energy accompanied by enhanced sediment supply from the east and along-axis sediment reworking. Persistent southward dipping of deltaic facies is consistent with the general pattern of delta progradation towards the strait axis observed in other sectors.

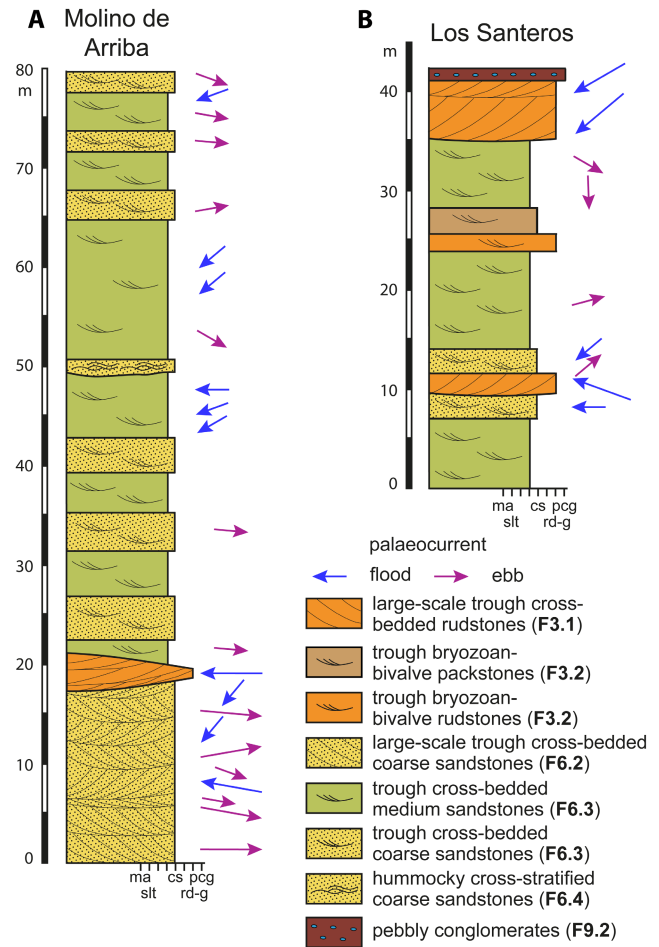


**FIGURE 14** Stratigraphic columns of the Molino de Arriba (A) and Los Santeros (B) sections in the western sector. Grain-size scale: cs, coarse sand; Ma, marl; pcg, pebbly conglomerate; rd-g, rudstone-granule conglomerate; slt, silt. Arrow length corresponds to the size of the cross-bedding (large or small-medium scale).

#### 4.2.4 | Western sector

##### *Molino de Arriba section*

The base of this section crops out on the righthand slope of the Alias river valley near the remains of the Molino de Arriba mill (Figure 2) and corresponds to the lower part of the section described by Dabrio (1987). The Pliocene rocks overlie Messinian marlstones at the north-western end of the outcrop. The lower part of the section consists of a 19 m thick package of coarse sandstones (F6.1) rich in bioclasts (Figure 14A), concentrated in some beds and lenses at the base of trough cross-beds forming rudstones. Bioclasts also concentrate in burrows. Coralline algal fragments are frequent in the lower 6.5 m together with calcitic bivalves, bryozoans and echinoids, which are the main bioclasts in the rest of the interval. These deposits show medium to large-scale trough cross-bedding (up to 5 m high and tens of metres wide) and medium-scale planar cross-stratification (F6.1). The prevailing foreset

migration points to the east in the lower 10 m whereas foresets indicate dune migration both to the east and west in the upper part of the package. The carbonate content increases to the north-west, where the laterally equivalent deposits can be described as packstones/rudstones (F3.1) (calcarenites in Dabrio, 1987). After a lens-shaped body of large cross-bedded rudstones (F3.1), up to 7 m in thickness, the succession continues with 60 m of alternating packages, several metres thick, of medium and coarse sandstones (F6.2), with varying (rare to abundant) bioclastic content and lenses of granule to pebble conglomerates. Lenses of shell concentrations with irregular bases also occur dispersed in the sandstones. Bidirectional (east–west) simple small to medium-scale trough/planar cross-bedding and ripples can be observed. At 50 m from the base of the section, an interval of coarse sandstone with granules and pebbles, rich in bioclasts, 1.5 m thick, shows an erosive base and hummocky cross-stratification at its top (F6.4).

#### *Los Santeros section*

This section is in the Los Santeros ravine some 300 m south-east of the top of the Molino de Arriba section (Figure 2) and is laterally equivalent to the upper part of the latter section. It consists of alternating packages, several metres thick, of medium and coarse sandstones with rare to abundant bioclasts and lenses of granule conglomerates (F6.2) (Figure 14B). The sandstones intercalate packstone and rudstone bedsets, 1.5–6 m in thickness (F3.2). All lithologies show simple small to medium-scale trough cross-bedding pointing eastwards and westwards, except for two rudstone intervals (F3.1) at 10 m from the base and in the upper part, which show large-scale trough cross-bedding pointing westward. The top of the succession is a pebbly conglomerate with quartzite clasts from the Betic basement at the northern margin of the basin (F9.2).

#### *Architecture and palaeocurrents*

The internal architecture of the about 90 m thick strait succession in the western sector is dominated by siliciclastic sandy simple cross-stratified bodies, with intercalated carbonate-rich intervals in the upper part. Large cross-bedding with tangential foresets, locally changing to planar, dominate the lower and upper part of the succession (Figure 15A). Foreset inclination is between 15° and 28° and records dune migration over tens of metres. The rest of the section is pervasively dominated by smaller bidirectional simple dunes that exhibit a nearly symmetrical size and abundance distribution, slightly skewed towards west-oriented. Their tangential foresets are similar to the larger compound dunes although slightly gentler dipping (10–25°; Figure 15B). The bedset surfaces are planar and

dip 2–5°. The general palaeocurrent orientation of the cross-stratified bodies indicates a vertical change in their migration direction from east-dominated to asymmetrically/symmetrically bidirectional east–west, which is accompanied by a change in the size and type of the bedforms (occurrence of both trough and planar cross-bedding), and then to west-dominated migration of larger structures. The thick vertical accretion of these cross-stratified bodies within a narrow facies belt showing evidence of tidal signature (e.g. bidirectional foreset migration) is indicative of a dune-bedded zone (Longhitano, 2013) similar to those proposed for the eastern and central-east sectors.

## 5 | DEPOSITIONAL MODEL

Facies analyses, their spatiotemporal distribution in the study outcrops and palaeocurrent data indicate that the Lower Pliocene deposits at the north-eastern end of the Almería-Níjar Basin accumulated in the roughly ESE-WNW oriented Río Alías Strait (Figures 2 and 16). The internal architecture of the strait deposits in the study sectors, composed mostly of thick stacked cross-strata, provides evidence for a tidal-dominated strait setting, which includes bidirectional migration of simple and compound bedforms (see Section 4.2 for details). The presence of cross-stratified coarse-grained deposits (sand and gravel) with bimodal flow patterns (e.g. herringbone cross-stratification) has traditionally been considered diagnostic of tidal processes and settings (Dalrymple et al., 1992; Davis Jr., 2012) and used as an indicator of tidal action in ancient straits (Martín et al., 2009; Longhitano et al., 2012; Longhitano, 2018b; Telesca et al., 2020; Gardner & Dorsey, 2021). These diagnostic features also include larger-scale unidirectional foresets migrating in the direction of the main tidal current and superimposed smaller-scale cross-stratified bodies migrating in opposite directions under residual current (Figure 5B,C). Other sedimentary features indicative of a tidal signature in ancient straits (see Longhitano & Chiarella, 2020 for a review) found in the Río Alías Strait deposits are (1) cyclic and regular rhythms of lamina-scale and bed-scale segregation of siliciclastic and bioclastic components (heterolithic lamination/stratification) (Figures 5B,D and 7C,D), which are interpreted to represent the transition from the dominant tidal current to the ensuing slack water stage (Longhitano, 2011; Longhitano et al., 2012). In small and medium-scale crossed-beds, these heterolithic rhythms are relatively regular in size (Figure 7C); (2) cyclic changes represented by thickening-thinning laminasets in small to large-scale foresets (Figures 5B,D and 7C,D), which could correspond to spring/neap-like

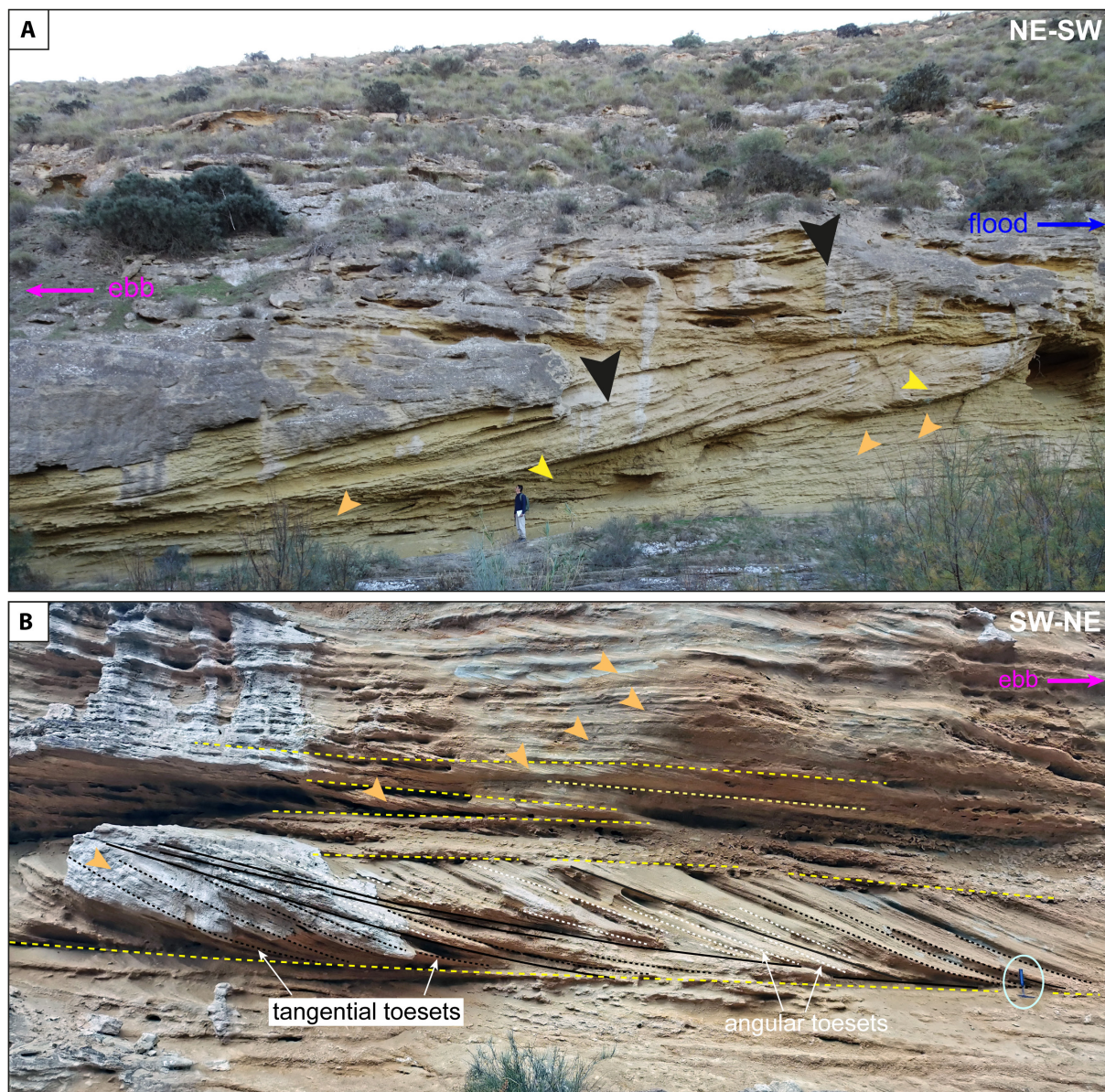


**FIGURE 15** (A) Outcrop view of the lower part of the Molino de Arriba section showing large-scale cross-bedding pointing eastward (black arrowheads) and overlying bedsets of smaller scale dunes migrating both eastwards (orange arrowheads) and westwards (yellow arrowheads). Person is 185 cm tall. (B) Close-up outcrop view of bedsets of small and medium (orange arrowheads) east-dominated dunes. Planar surfaces (yellow dotted lines) separating cross-beds also dip towards the east. Reactivation surfaces (black lines) and changes in the toeset morphology are also marked in a medium-scale dune. Hammer is 33 cm long.

tidal cycles as suggested in other ancient tidal settings with mixed siliciclastic-carbonate sedimentation (Longhitano et al., 2010; Longhitano, 2011; Longhitano et al., 2012); and (3) changes in foreset geometry from tangential to angular toesets (Figures 5C, 7A and 15B), which have been related to the accretion velocity resulting from accelerating and decelerating tidal currents, respectively (Chiarella, 2016).

Dalrymple (2023) has recently brought attention to the fact that meteorologically generated currents (atmospheric or wind-driven) may lead to sedimentary dynamics in straits similar to those referable to tidal

currents. Water level differences between the two ends of a strait pushed by these meteorological processes can potentially lead to reverse flows, especially in relatively short straits. As a consequence, the sedimentary record of these intermittent currents might generate sedimentary features similar to tide-generated ones, such as bidirectional foreset migration, reactivation surfaces and rhythmic bundles. However, although the meteorologically generated currents are observed and/or modelled in many modern straits (e.g. Asinelli, Bering, Lombok, Mackinac, Skagerrak, see Dalrymple, 2023 and references therein), their proven impact on the

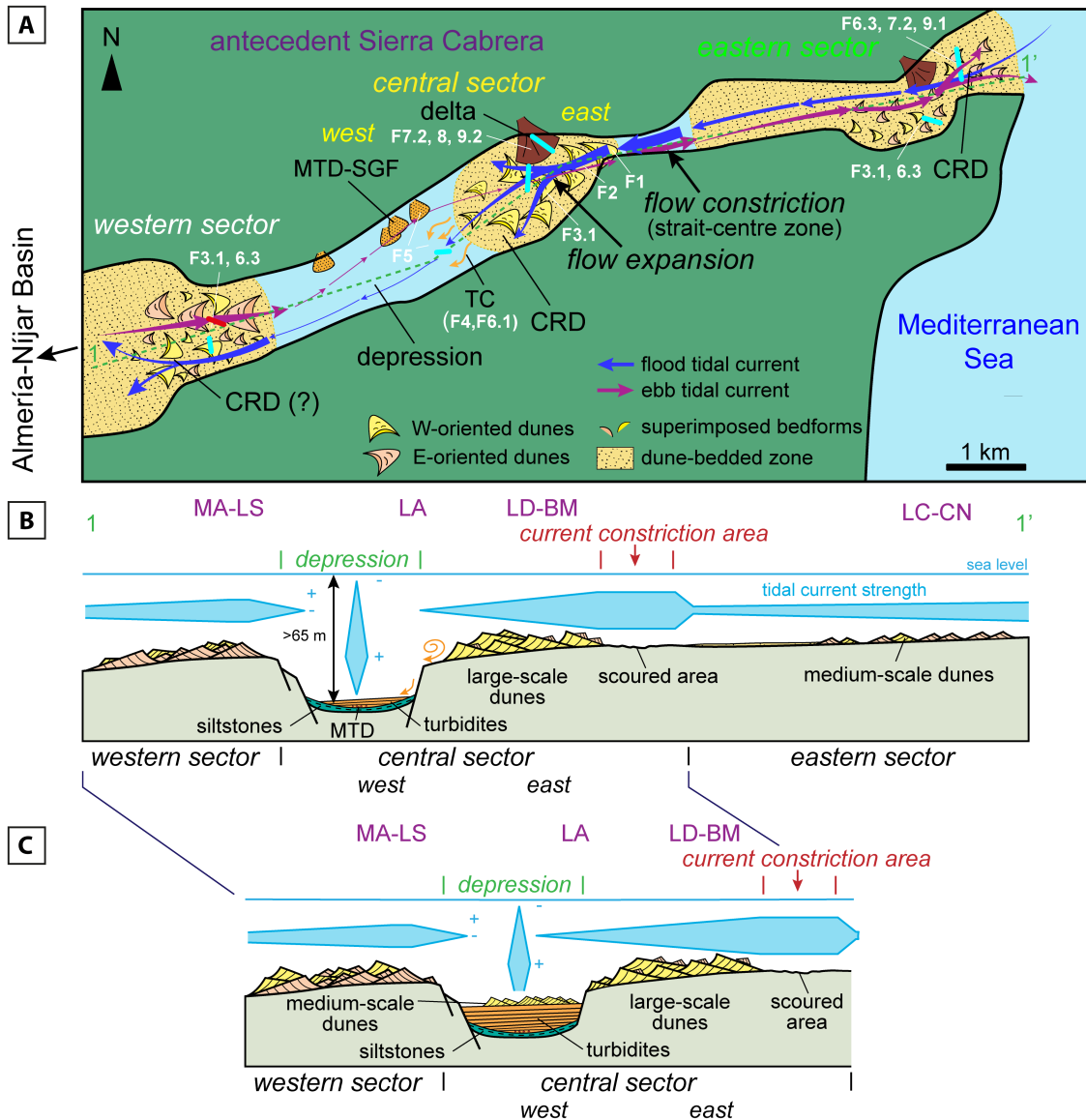


**FIGURE 16** (A) Sketch illustrating the reconstruction of the Río Alías Strait during the Early Pliocene based on preserved outcrops (see Section 5 for details). The pathway of the strait was probably controlled by tectonics as it roughly has the same orientation as the sinistral N45E Carboneras and the dextral E–W to ENE–WSW Polopos/South Cabrera strike-slip fault systems. A dune-bedded strait zone is the best represented in the strait. The widening of the strait towards the central sector and eastern and western exits promoted flow expansion of tidal flood currents and the formation of constriction-related deltas (CRD). MTD, mass-transport deposits; SGF, sediment gravity flow deposits; TC, turbidity currents. (B) Conceptual cross-section (see location in A marked by the green dashed line from 1 to 1') showing the location of the medium- and large-scale dunes in the different strait sectors. Note the absence of bedforms both on the depression between the central-west and central-east sectors (enlargement of cross-sectional strait area) and the strait-centre zone between the central and eastern sectors (narrowing of cross-sectional strait area). BM, Barranco del Malo section; CN, Carboneras Norte section; LA, La Arbolea section; LC, Loma de la Cañada section; LD, Llanos de Don Antonio section; LS, Los Santeros section; MA, Molino Arriba section. (C) Conceptual cross-section showing how the progressive fill-up of the central-west depression led to the decrease in the cross-sectional area and progradation of dunes towards the west. In the western strait exit, large-scale dunes were moved by the flood (westward) current likely forming a CRD.

ancient record remains uncertain and there are no clear diagnostic sedimentological criteria to separate their effects from those of tidal currents. In the case of the Río Alías Strait, if the modern climate conditions at the Carboneras coast (Figure 1; Molina et al., 2019) are considered as an analogue (e.g. about 24 stormy days

per year of 1–4 days duration, of which only two events are of moderate or higher energy) it would be expected that the relatively short duration and the number of storm events and related reversal wind-driven currents would have generated more irregular cycles (e.g. heterolithic bundles) than those observed in the strait record

(Figures 5B,D and 7C,D). In addition, the fair-weather periods between storms would have led to bioturbation of the dune foresets, in particular cross-bedded surfaces, which is not observed either. By comparison with modern examples, the occurrence of wind-driven generated currents in the Río Alías Strait cannot be discounted, but their imprints in the preserved record are uncertain. Therefore, even within a microtidal setting such as the Mediterranean Sea (Chiarella & Longhitano, 2012; Longhitano et al., 2012), tidal currents played a major role in the distribution and accumulation of mixed carbonate–terrigenous deposits in the Río Alías Strait.

This interpretation is overall in line (see further discussion in Section 6.1) with the subdivision of the strait into discrete sedimentary zones following Longhitano (2013) model, which is based on the distinctive hydrodynamics across straits and is partitioned into four adjacent depositional zones: (1) the strait-centre zone that acts mainly as a by-pass zone; it corresponds to the strait zone with the most reduced cross-sectional area and thus the strongest current amplification and acceleration, which merge into (2) the dune-bedded strait zone (or CRDs of Dalrymple, 2023) where a bedform continuum develops as a function of the current strength and represents the main depocentre; (3) the strait-end zone (or deep basins between constrictions of Dalrymple, 2023), which commonly represents the downstream continuation of the dune-bedded zone and hosts the finest-grained sediments; and (4) the strait-margin zone, which includes point-source sediment supply to the strait; depending on the margin gradient it comprises a variety of sub-environments (e.g. fan deltas, river deltas, canyons and turbidite channels). The vertically stacked (75–150 m thick), coarse-grained (sand and conglomerate) carbonate and mixed carbonate–terrigenous successions exhibiting large-scale cross-stratification in the eastern, central-east and western sectors are indicative of the existence of a dune-bedded zone (see Section 4.2 for details), which is best represented in the Río Alías Strait. The cross-bedded facies belt shows an elongated distribution along the main transport pathways deduced from palaeocurrent analysis. Coarse-grained terrigenous inputs through fluvial sources at the northern margin, mass-transport deposits and sediment gravity flow deposits, especially in the eastern and central sectors are indicative of strait-margin facies. The finest-grained sediments in the Río Alías Strait occur in the central-west sector, which can be assigned to a relative deep-water depression separating the dune-bedded zones in the central-eastern and western sectors.

The tidal-driven depositional model developed for the Río Alías Strait corresponds to an elongated strait, with punctual narrows in map view, with multi thresholds along an ESE-WNW longitudinal profile and a simple channel

with axial-dominated deposition and local lateral supply in transverse section (Figure 16). Westward-directed flood tidal currents from the Mediterranean Sea were amplified and accelerated owing to topographic constraints (both in width and depth) and the decrease of the strait cross-section in the easternmost part of the central-east sector and in transition to the eastern sector, which represents the strait-centre zone (Figure 16). The very coarse-grained barnacle rudstones (F1) with large-scale cross-bedding in the central-east sector (Llano de Don Antonio section; Figures 2, 4A,B and 10A) suggest peak current velocities of at least 130 cm/s through this narrow area (Ashley, 1990). Current velocity might have been even higher at the area of maximum constriction leading to a dune-bare sea-floor with patchy gravelly deposits as it occurs in modern tide-dominated straits such as the Cook Strait, Messina Strait and Minas Passage (Proctor & Carter, 1989; Shaw et al., 2012; Longhitano, 2018a). Downstream (westward) from the strait-centre zone, flood tidal currents decelerated because of flow expansion due to unconfinement and led to the development in the central-east sector of the dune-bedded zone with the largest bedforms (Figures 5A, 11 and 10A). Palaeocurrent data in this sector show a radial pattern (Figure 11) that suggests a topographically-controlled flow expansion to the west leading to the deposition of a lobate body (e.g. tidal-flood delta in Reynaud et al., 2006) or CRD (sensu Dalrymple, 2023) formed by the vertical stacking of mostly 3D simple and compound dunes. Although a progressive down-scaling of the ebb-moved dunes would be expected towards the west, field data suggest a rather abrupt change to fine-grained facies accumulated in the central-west sector (Figure 16). This change could result from an increase in cross-sectional area due to strait widening and/or most likely due to the existence of a deeper-water depression, as in the case of the Tortonian Zagra Strait in the Betic Cordillera (Puga-Bernabéu et al., 2022; Figure 16). The strike-slip fault-controlled course of the strait (Figure 2) very likely conditioned its partitioning in horst and grabens that exerted a major control on tidal current hydrodynamics. Such thresholds also occur in modern straits located in transform margins such as the Queen Charlotte Sound–Johnstone Strait (Dossier et al., 2021) or the Turkish Straits System (Dardanelles Strait, Sea of Marmara and Bosphorus Strait; Gökaşan et al., 2008; Ferrarin et al., 2018). The deep-water depression hosted mass-transport deposits sourced from the northern margin and sediment gravity flows sourced from the large-scale dunes in CRD to the west and incorporated in the depression, both lacking evidence of tidal current (Figures 13 and 16). The turbiditic flows are interpreted to have originated from the collapse of dune foresets during current-reduced activity or due to flow expansion as a consequence of increased accommodation space at the end of the CRD.

The relative narrowing of the strait at the western sector caused the same effect of tidal current amplification on the ebb current as in the eastern entrance, generating the dominant eastward-migrating large-scale dunes and forming a likely CRD in the transition to the depression of the central-west sector, with subordinated west-migrating large bedforms (Figures 14, 15A and 16). Decelerated flood currents in the depression of the central-west sector accelerated again when reaching the western-sector funnel, leading to the nearly symmetrical bidirectional (east–west) pattern in the migration of small and medium-scale bedforms. Towards the eastern strait exit and after flowing through the strait-centre narrowing, tidal ebb currents decelerated and moved simple small to medium-scale dunes forming another CRD (Figure 16). In contrast to the CRD west of the constriction, the elongated morphology of the eastern CRD likely resulted from the gradual increase in accommodation space. In this CRD, eastward-migrating dunes are concentrated in its central part facing the eastward constriction exit, while oppositely migrating dunes located preferentially at the strait margins (Figures 9 and 16). The resulting bidirectional palaeocurrent pattern suggests that the eastern sector was located in the transition to the strait-end zone (Longhitano & Chiarella, 2020), which in this part of the strait would be located further east. High terrigenous content in the dune sediments from the eastern sector suggests the presence of a point-source sediment supply likely similar (fan delta or delta) to that in the central-east sector (Barranco del Malo section; Figures 9, 10B and 16).

Upward facies changes in the La Arboleja section (Figure 13) record a shallowing upward succession and the increased influence of eastward-directed currents. These deposits are interpreted as the progressive infilling of the central depocentre by sediment sourced from downcurrent extension and progradation of the large CRD to the east (Figure 16C). As a consequence of the decreasing accommodation over the depression, flow expansion at the western constriction waned and the formation of the CRD was hindered. Large-scale westward-migrating (flood-dominated) dunes could indicate intermittent reactivation of the CRD.

## 6 | DISCUSSION

### 6.1 | Sedimentary dynamics and comparison with existing case studies

Straits are sedimentary systems with a wide range of dimensions and morphologies characterised by distinctive sedimentary dynamics where current energy changes, resulting from variations in the hydraulic cross-sectional area, exert the main control on the sediment distribution pattern along the strait axis. The fourfold general facies model of

Longhitano (2013), which was initially proposed for assessing tectonically confined tidal straits, can be generally applied to modern and ancient tide-dominated, meteorologically or current-dominated straits (see Rossi et al., 2023a, 2023b), although some modern examples deviate from this model (Dalrymple, 2023). Within the ancient sedimentary record, the classic model has been expanded by the better characterisation of strait-margin environments (Longhitano & Steel, 2016; Rossi et al., 2017; Telesca et al., 2020; Gardner & Dorsey, 2021; Longhitano et al., 2021; Dalrymple, 2023). A variation in the along-axis facies tracts was described by Puga-Bernabéu et al. (2022) in the Zagra Strait (early Tortonian, Betic Cordillera). Here, a deeper-water depression occupied the relative position of the strait-centre zone within the strait system while the dune-bedded zone occupied the relative sills. Such deeper-water depression favoured current expansion and deceleration due to enlargement of the strait cross-sectional area and, as in the case of the sill-located strait-centre zone sensu Longhitano (2013), it was an area of reduced sediment deposition, but not due to erosional and bypass processes. The Río Alías Strait holds both the sill of the classic model (Longhitano, 2013) and the depression of the Zagra Strait (Figure 13), very likely due to its tectonically controlled configuration. As in the Zagra Strait, field data suggest the existence of a relatively deep-water depression (intra-strait depression; Dalrymple, 2023) in the Río Alías Strait separating the western and the central-east sectors (Figure 16), which led to dissipation of tidal current energy. However, the increase of the cross-sectional area in the Río Alías Strait was most likely due only to an increase in water depth (Figure 16) and not to a combination of water depth and strait width as in the Zagra Strait (Puga-Bernabéu et al., 2022). In both considered straits, there is a sharp transition from the dune-bedded strait zone to the depression, which suggests the trough was fault-bounded (Figure 2). In the Río Alías Strait, outward from the sill between the central-east and eastern sectors, sediment transport departs towards opposite directions (roughly east–west), but with an asymmetry in the development of the CRD in both areas of flow expansion. The largest dunes formed due to the Mediterranean tidal flood at the western side of the constriction (Figures 5A, 11, 12A and 16) while to the east bedforms were smaller. The identification in the fossil record of the precise location of the maximum current amplification and acceleration within the strait-margin zone is not an easy task, as erosion due to bottom stress maxima dominates this zone and it can be quickly buried by thick sequences of cross-stratified deposits and other sediments (Longhitano, 2018b; Longhitano & Chiarella, 2020). The location of the Río Alías Strait throat is supported by field evidence and it probably corresponds to the shallowest and narrowest strait area (Figure 16). The threshold of erosion of submarine bedrock by tidal currents suggests they may abrade the seafloor but

it is unlikely that they erode it (Mitchell et al., 2013). In the Río Alías Strait, however, erosion could have been favoured by the soft nature of the bedrock (Messinian marls; Figures 3 and 10) and the existence of a scour depression (hollow) along the eastern sill as in the modern Golden Gate Inlet, Hayasui Strait, Northumberland Strait and Minas Passage (Kranck, 1972; Ikehara & Kinoshita, 1994; Barnard et al., 2006, 2013; Shaw et al., 2012; Dalrymple, 2023) cannot be excluded.

## 6.2 | Water depth estimations in the Río Alías Strait

Water depth is an important parameter that influences the sedimentary dynamics and facies distribution in straits (e.g. location of constrictions and enhanced flows and long-term dune size changes) and can be largely variable along their lengths (Dalrymple, 2023). The scaling of subaqueous dune foreset height ( $H$ ) with depth is still the best approach to make first-order estimates of palaeowater depth ( $D$ ) in the ancient record (see Bradley & Venditti, 2017). Widely used  $H$  versus  $D$  relationships are those of Yalin (1964) ( $H=0.167D$ ) or Allen (1982) ( $H=0.086D^{1.19}$ ) (Bradley & Venditti, 2017). Based on Allen's (1982) scaling relationships ( $H=0.086D^{1.19}$ ), the average foreset heights (3 m in the western sector and 6 m in the central-east sector) of the large-scale dunes in the Río Alías Strait yield strait palaeowater depths of *ca* 30–50 m in the dune-bedded zone. Bradley and Venditti's (2017) approach ( $D=6.7H$  and their uncertainty range) suggests palaeowater depths of 20–40 m for the Río Alías Strait within an uncertainty range boundary of 50% (scaling factor of 4.4–10.1) of 13–60 m. The largest simple dunes (*ca* 10 m in height) would yield maximum palaeowater depths of 67 m in the dune-bedded zone. It is worth highlighting that these estimates might be biased (up to 40%; Longhitano et al., 2014), as the foreset height must be considered the minimum preserved dune height. Within the ancient record, the Río Alías Strait was likely deeper than the late Miocene Midway strait (*ca* 25 m; Gardner & Dorsey, 2021) in the south-western USA and slightly shallower than the Mediterranean Tortonian–Messinian Logudoro seaway, which might have reached *ca* 150 m at the end of its transgressive infilling (Telesca et al., 2020). Water depth estimates in the Río Alías Strait are on the order of other microtidal Mediterranean straits, such as the lower Pleistocene Mediterranean Catanzaro (30–80 m; Longhitano et al., 2014) and Messina (35–75 m; Longhitano, 2018b) straits. Note that in these straits, the authors took into account an increment between 30 and 40% of the foreset height measured in the outcrops to obtain a reliable estimate of the primary tidal dune. In

a closer realm within the Betic Cordillera, marine straits connecting the Mediterranean Sea and the Atlantic during the Miocene host larger dunes (foreset height commonly between 10 m and 30 m; Martín et al., 2001, 2009, 2014; Betzler et al., 2006; Puga-Bernabéu et al., 2022) and, therefore, they were deeper (i.e. average palaeowater depths of *ca* 70–200 m). Compared with modern straits, water depth approximations for the Río Alías Strait are similar to the Golden Gate Inlet where large-scale dunes up to 10 m high move coarse sand to small pebbles along a marine corridor *ca* 5 km long and 1.5–3.5 km wide at water depths of 30–106 m (Barnard et al., 2006, 2013, 2013). In addition, the CRD at the western exit of the scoured strait throat where the largest dunes developed is akin to the Río Alías Strait analogue.

Water depth is critical in shallow-water (<100 m water depth) straits as high-amplitude sea-level fluctuations (e.g. during the Late Pleistocene; see Rossi et al., 2023a, 2023b and Dalrymple, 2023 for a review in modern straits) lead to strait emersion and exposure to subaerial processes during relative sea-level falls (Emmel & Curray, 1982), and fluvio-estuarine to estuarine sedimentation during the later transgression (Kranck, 1972; Roberts et al., 2011). During the Early Pliocene, high-frequency sea-level fluctuations were in the range of 20–30 m (Miller et al., 2005; Rohling et al., 2014). Diagnostic features of subaerial exposure (such as soil intervals and/or karstification surfaces) are not observed in the study area. Therefore, sea-level variations did not produce clear signs of exposure or they were not high enough to expose the seafloor of the Río Alías Strait in subaerial conditions. However, sea-level drops of such magnitude might have impacted the sedimentary dynamics along the strait by changing the optimal depth for the generation of large-scale bedforms (Anastas et al., 2006). The sharply erosional reactivation surfaces that separate sets of large-scale dunes in the central CRD (Figures 5A, 11 and 12) might have formed during periods of relative sea-level falls. High-energy currents resulting from the decreased cross-sectional area could have eroded and bypassed sediment of underlying dunes and locally generated upper-stage plane beds (Figures 5A and 12B). These plane beds represent the transition to large-scale tidal bedforms in higher accommodation conditions such as in the ancient Messina Strait (Longhitano, 2018b). Lowstand conditions could have also favoured the formation of sediment gravity flows filling the depression.

## 6.3 | Grain composition and provenance in the Río Alías Strait

Compared with wide straits and seaways, narrow straits (<35 km, Rossi et al., 2023b) are less prone to

be enriched in carbonate sediments due to the shorter distance from the terrigenous sources at their margins (Dalrymple, 2023), especially if they are in tectonically active margins bounded by faults. However, the Río Alías Strait deposits comprise a suite of sedimentary facies that indicate biogenic carbonate and terrigenous sources, which are mixed into various proportions along and across the strait seafloor. A mixed carbonate-terrigenous (siliciclastic) sediment composition is a widespread feature found in the majority of the ancient (Miocene and Pleistocene) strait deposits in the Mediterranean region (among others, the North Betic, Dehesas de Guadix and Zagra straits in the Betic Cordillera; the Bonifacio Strait between Corsica and Sardinia; the Logudoro seaway in Sardinia, the Catanzaro, Messina and Siderno straits in the Calabrian arc); (Martín et al., 2001, 2009, 2014; Betzler et al., 2006; Braga et al., 2010; Chiarella et al., 2012; Longhitano et al., 2012, 2014; Longhitano, 2018b; Reynaud et al., 2013; Rossi et al., 2017; Telesca et al., 2020; Puga-Bernabéu et al., 2022) and the palaeo-Gulf of California (Gardner & Dorsey, 2021; O'Connell et al., 2021), as well as in other older straits, such as those in the Ager Basin (central Pyrenees) during the early Eocene (Olariu et al., 2012) or in the Cortina–Tofane area (Dolomites) during the Late Triassic (Gattolin et al., 2013). The nature of terrigenous sediments in the Río Alías Strait deposits indicates that they were mainly sourced from the hinterland basement rocks at the northern margin (see Section 6.3) and were introduced into the strait via fluvial and alluvial inputs (Figure 16). Minor terrigenous supply came from erosion of the basement on the strait bottom, especially in the central-east sector. Promoted by the short distance between the strait margins, terrigenous sediments were soon reworked by tidal currents, being hydraulically and compositionally mixed (sensu Chiarella et al., 2017) with skeletal carbonate particles and incorporated into the bedforms moving along the strait.

The biogenic carbonate fraction is variable along the Río Alías Strait, being more abundant in the central and eastern sectors (Figures 9, 10, 13 and 14). Whereas the abundance of carbonate in the central sector contrasts with its distribution in some modern straits with mixed carbonate-terrigenous sedimentation such as the Malacca and Singapore straits, where carbonate content increases towards the strait exits (Keller & Richards, 1967; Dalrymple, 2023). The biogenic composition dominated by bivalves, bryozoans and locally by balanids (facies F1, F2 and F3) points to a dominant heterozoan skeletal carbonate production of suspension-feeding organisms. Tidal currents likely promoted these benthonic communities by favouring the supply and mixing of nutrients. Although

fragmented and abraded, abundant coarse-grained balanid remains in facies F1 and F2 point to a parautochthonous carbonate factory attached to the strait walls close to or at the maximum constriction area (Figure 16), very likely at <50 m depth (Coletti et al., 2018). This is consistent with depth estimates from dune foresets heights (see above). A more ubiquitous bryozoan/bivalve-dominated carbonate factory could have developed either on the dune surfaces (Reynaud et al., 2006; James et al., 2014) or on narrow ramps (e.g. ramp-type wedges in the Pleistocene Messina Strait; Longhitano, 2018b) at the strait margins distant from siliciclastic inputs. High-energy currents along the Río Alías Strait also promoted the proliferation of burrowing echinoids (*Scolicia*) on the highly mobile sandy and gravelly dune sediments as in other Mediterranean straits (e.g. Catanzaro and Siderno straits; Longhitano et al. 2014; Rossi et al., 2017).

Most terrigenous clasts in the Río Alías Strait deposits are sourced from the antecedent relief of Sierra Cabrera at the northern strait side, whereas clast provenance from the Cabo de Gata volcanic reliefs is negligible. Sierra Cabrera is the youngest upland of the Betic basement in South-East Spain (Braga et al., 2003). Although the submarine uplift of its antecedent relief conditioned the distribution of deep-water sediments in the southern part of the Vera Basin during the latest Tortonian (Braga et al., 2001), the Sierra Cabrera first emerged in the late Messinian (Braga et al. 2003). The nature of clasts in the Barranco del Malo section reflects the continued uplift of the Sierra Cabrera during the Early Pliocene and reveals the sequence of exhumation of the stack of complexes comprising the Betic basement and the incision of the drainage system in successively deeper tectonic units. Showing an inverted stratigraphy, the lower 14.5 m of the delta deposits in the section contain clasts from the Messinian infill of the Almería-Níjar Basin and from the Maláguide and Alpujarride complexes, the two upper complexes in the Betic-basement pile in Sierra Cabrera (Rondeel, 1965; Weijermars, 1991). In contrast, from that level upward in the section, most clasts are quartzites sourced in the Nevado-Filábride Complex which is the lower complex of the Betic pile and builds the nucleus of Sierra Cabrera (Rondeel, 1965). Quartzites and minor micaschists and metabasites from the Nevado-Filábride Complex are the main terrigenous components in the delta of the Loma de la Cañada section and in the delta deposits on top of the strait infill in all sectors, which eventually caused its closure. The regressive strait-fill succession of the Río Alías Strait is coherent with the closure pattern observed in the straits that connected the Atlantic Ocean and the Mediterranean Sea through the Betic Cordillera during the Miocene (Martín et al., 2001, 2009, 2014; Betzler et al., 2006; Braga et al., 2010,

Puga-Bernabéu et al., 2022) as a result of the progressive tectonic uplift of the cordillera.

## 6.4 | Palaeogeographical evolution leading to the strait configuration

The northward, left-lateral movement of the Cabo de Gata terrain along the CFZ (Keller et al., 1995; Scotney et al., 2000; Rutter et al., 2012, 2014) approached the emergent uplands of the Cabo de Gata volcanics to the antecedent relief of Sierra Cabrera, narrowing the seaway connecting the Almería-Níjar Basin with the main Mediterranean during the Late Miocene. Although movement continues today at low rates (Moreno et al., 2015; Echeverría et al., 2015; Masana et al., 2018), the main CFZ movements began 11–12 Ma and ended about 6 Ma, that is, at the end of the early Messinian, according to evidence provided by the stratigraphy of volcanic rocks related to the fault (Rutter et al., 2014). The Sierra Cabrera anticlinal high of Betic metamorphic basement was itself uplifting and drifting eastward along the dextral-oblique Polopos fault zone (Giaconia et al., 2012, 2014). The convergence of both blocks narrowed the connection of the Almería-Níjar Basin with the open Mediterranean Sea in a period of complex palaeoceanographic evolution of this area. Although there is evidence of submarine highs and potentially emergent antecedent uplands of the Sierra Cabrera (Braga et al., 2001), the lower Messinian marls crop out around the Sierra de Cabrera basement with no laterally equivalent shallow-water deposits, indicating that deep-water marine conditions prevailed in the area. The emersion of the upland took place later, in the late Messinian (Braga et al., 2003) and continental to shallow marine deposits with clasts derived from the north fringe of the southwestern slope of Sierra Cabrera were produced (Fortuin & Krijgsman, 2003; Aguirre & Sánchez-Almazo, 2004; Omodeo Salé et al., 2012). In contrast, there is evidence of emergent volcanic highs at the southern margin of the seaway in the early Messinian (Martín et al., 1996, 2003, 2004). Between marl deposition in the early Messinian and the accumulation of strait deposits in the Early Pliocene, the Mediterranean Basin underwent a major stage of sea-level fall related to the MSC (Hsü et al., 1977; Rouchy & Caruso, 2006). In the Río Alías area, the erosion surface underlying the strait deposits is related to the basin emersion during the Messinian crisis, and the succession indicates that the marine reflooding took place when a linear depression was already configured. This depression probably was a fluvial valley laterally connected to the Almanzora-Alías-Garrucha canyon, which cuts the slope and continental

shelf off the Alías river mouth and was already incised in the late Messinian (Ercilla et al., 2022).

The Río Alías strait deposits overlie Messinian sedimentary rocks and Cabo de Gata volcanics at both sides of the CFZ system and are delimited by NE–SW faults of this system and E–W faults. This indicates that the linear depression was also conditioned by the E–W to ENE–WSW fault systems bounding the Almería-Níjar Basin to the north (Polopos fault zone/South Cabrera fault; Figure 2; Harvey & Mather, 2015; Giaconia et al. 2012), which accommodated the eastward movement of the Sierra Cabrera block. The present-day distribution of rocks outcropping along the CFZ indicates that it is structured in a series of subsiding areas and topographic highs (Boorsma, 1992; Bell et al., 1997). This pattern probably caused the lateral occurrence along the strait area of narrow highs in which confined currents accelerated and deeper depocentres in which flows expanded and decelerated, driving the spatial distribution of facies observed.

## 7 | CONCLUSIONS

During the Early Pliocene, the Río Alías Strait was a *ca* 13 km long and 0.5–2 km wide, WNW to ESE oriented marine corridor that connected the microtidal open Mediterranean Sea and the north-eastern margin of the Almería-Níjar Basin in the eastern Betic Cordillera (South-East Spain). This strait was structurally shaped by the transpressive sinistral N45E Carboneras fault and the dextral E–W to ENE–WSW Polopos/South Cabrera strike-slip fault systems. The northward displacement of the Cabo de Gata volcanic terrain along the fault and the emergence of the fault-bounded antecedent relief of Sierra Cabrera narrowed the north-eastern end of the Almería-Níjar Basin. A linear depression following faults of these systems cut the Messinian rocks of the Almería-Níjar Basin and Cabo de Gata volcanics. This linear depression probably was a fluvial valley during the MSC and was reflooded in the Early Pliocene creating a strait with subsiding depressions and topographic highs. The stratigraphic succession of the strait deposits records the effect of tidal current amplification owing to the narrowing of the cross-sectional area. The following are the major conclusive remarks achieved with the present study.

1. The strait succession is composed of 10 facies types and 12 subtypes, which reflect the compositional mixing of biogenic carbonates and terrigenous sediments under the effect of tidal currents. Terrigenous sediments were mainly sourced from the antecedent relief of Sierra Cabrera at the northern strait side

- and accumulated principally in fan deltas and river deltas. The biogenic carbonate fraction includes a heterozoan association of suspension-feeders (balanids, calcitic bivalves and bryozoans) that benefited from the high-energy hydrodynamic conditions in the strait and formed carbonate factories at the strait walls, narrow ramp-type wedges, or developed on bedform surfaces.
- The highest current acceleration is recorded by erosion of the underlying marly basement and conspicuous, nearly monomictic, pebble-size, cross-bedded barnacle rudstone facies. Depositional neptunian dykes observed in this facies point to early lithification of the rudstone at the strait floor under the high-energy current regime and opening of fractures in a locally extensive context.
  - The main facies correspond to large-scale cross-stratified bodies up to 15 m thick, which form simple and compound, mostly 3D tidal dunes. The thick (up to 150 m) vertical accretion of these cross-stratified bodies is indicative of dune-bedded zones developed in different sectors along the strait, where cross-bedding records the migration of dunes in opposite east–west directions. Only larger-scale dunes exhibit a certain degree of asymmetry in palaeocurrent directions while palaeocurrents in medium-scale dunes are mostly symmetrical.
  - The Río Alías Strait shows that small straits can develop complex and pronounced lateral and vertical facies changes over extremely short distances. The multi-threshold strait includes two relative sills separated by a deeper-water depression (>65 m deep based on estimates from the dune foreset height) located in the central part. The narrowest topographic constraint was in the central-east sector. Large-scale dune migration was hindered because of the presence of a depression and the main constriction in the strait. On the contrary, dune fields expanded at the two opposite strait enlargements, forming CRDs. The depression was initially fed by local lateral supply via mass-transport movements and sediment gravity flows from the east until the filling of the depocentre created favourable conditions for tidal sediment reworking on the seafloor.
  - At the main strait narrowing, westward-directed flood tidal currents from the Mediterranean Sea were first amplified and then decelerated downcurrent forming a lobated body (or CRD) due to unconfinement and flow expansion. A bedform scaling to smaller east-dominated dunes occurred upstream towards the eastern strait sector, where they formed an elongated CRD due to a progressive decrease in accommodation. Ebb-current amplification at the relatively western narrowing and subsequent flow expansion in the transition

to the central depression also generated an elongated CRD.

- The sedimentary evolution of the Río Alías Strait exemplifies that narrow, small straits are relatively ephemeral geological features and highly conditioned by the local tectonic context. The nature of the clasts sequentially accumulated in deltaic environments at the northern side of the Río Alías Strait reflects the continued uplift of Sierra Cabrera during the Early Pliocene and reveals the sequence of exhumation of the stack of complexes comprising the Betic basement. This progressive uplift favoured delta southward progradation over the strait axis in all sectors, eventually leading to strait closure.

### ACKNOWLEDGEMENTS

This paper has been supported and funded by the research projects SECAMARA (PGC2018-099391-B-100) of the Spanish Ministerio de Ciencia e Innovación and TRANSCARB (A-RNM-438-UGR20) of the Consejería de Economía, Conocimiento, Empresas y Universidad of the Junta de Andalucía, and the research group RMN190 of the Junta de Andalucía. We thank Javier Jaimez (Centro de Instrumentación Científica, Universidad de Granada) for their assistance with the drone flights and data processing. We thank S.G Longhitano for his comments and editorial work. We appreciate valuable insights by reviewers R.W. Dalrymple and D. Chiarella, who helped to improve an earlier version of this manuscript.

### CONFLICT OF INTEREST STATEMENT

The authors declare no conflicts of interest.

### DATA AVAILABILITY STATEMENT

The data that support the findings of this study are available from the corresponding author upon reasonable request.

### ORCID

Ángel Puga-Bernabéu  <https://orcid.org/0000-0002-6420-9167>

### REFERENCES

- Aguirre, J. (1998) El Plioceno del SE de la Península Ibérica (provincia de Almería). Síntesis estratigráfica, sedimentaria, bioestratigráfica y paleogeográfica. *Revista de la Sociedad Geológica de España*, 11, 297–315.
- Aguirre, J. & Sánchez-Almazo, I.M. (2004) The Messinian post-evaporitic deposits of the Gafares area (Almería-Níjar basin, SE Spain). A new view of the “Lago-Mare” facies. *Sedimentary Geology*, 168, 71–95.
- Allen, J.R.L. (1982) Sedimentary structures: their character and physical basis, volume II. *Developments in Sedimentology*, 30B, 645.

- Anastas, A.S., Dalrymple, R.W., James, N.P. & Nelson, C.S. (1997) Cross-stratified calcarenites from New Zealand: subaqueous dunes in a cool-water, Oligo-Miocene seaway. *Sedimentology*, 44, 869–891.
- Anastas, A.S., Dalrymple, R.W., James, N.P. & Nelson, C.S. (2006) Lithofacies and dynamics of a cool-water carbonate eaway: mid-Tertiary, Te Kuiti Group, New Zealand. In: Pedley, H.M. & Carannante, G. (Eds.) *Cool-water carbonates: depositional systems and palaeoenvironmental controls*, Vol. 255. London: Geological Society, London, Special Publications, pp. 245–268.
- Ashley, G. (1990) Classification of large-scale subaqueous bedforms: a new look at an old problem. *Journal of Sedimentary Petrology*, 60, 170–172.
- Bardaji, T., Goy, J.L., Silva, P.G., Zazo, C., Mörner, N.A., Somoza, L., Dabrio, C.J. & Baena, J. (1997) The Plio-Pleistocene boundary in southeast Spain: a review. *Quaternary International*, 40, 27–32.
- Barnard, P.L., Hanes, D.M., Rubin, D.M. & Kvitek, R.G. (2006) Giant sand waves at the mouth of San Francisco Bay. *Eos*, 87, 1–3.
- Barnard, P.L., Erikson, L.H., Elias, E.P.L. & Darnell, P. (2013) Sediment transport patterns in the San Francisco Bay Coastal System from cross-validation of bedform asymmetry and modeled residual flux. *Marine Geology*, 345, 72–95.
- Barnard, P.L., Schoellhamer, D.J., Jaffe, B.E. & McKee, L.J. (2013) Sediment transport in the San Francisco Bay Coastal System: an overview. *Marine Geology*, 345, 3–17.
- Beelen, D., Wood, L.J., Zaghoul, M.N., Cardona, S. & Arts, M. (2022) Channel, dune and sand sheet architectures of a strait-adjacent delta, Rifian Corridor, Morocco. *Geological Society, London, Special Publications*, 24, 51–66.
- Bell, J.W., Amelung, F. & King, G.C.P. (1997) Preliminary late quaternary slip history of the Carboneras fault, southeastern Spain. *Journal of Geodynamics*, 24, 51–66.
- Betzler, C., Braga, J.C., Martín, J.M., Sanchez-Almazo, I.M. & Lindhorst, S. (2006) Closure of a seaway: stratigraphic record and facies (Guadix basin, Southern Spain). *International Journal of Earth Sciences*, 95, 903–910.
- Boorsma, L.J. (1992) Syn-tectonic sedimentation in a Neogene strike-slip basin containing a stacked Gilbert-type delta (SE Spain). *Sedimentary Geology*, 81, 105–123.
- Borque, M.J., Sánchez-Alzola, A., Martín-Rojas, I., Alfaro, P., Molina, S., Rosa-Cintas, S., Rodríguez-Caderot, G., de Lacy, C., Avilés, M., Herrera-Olmo, A., García-Tortosa, F.J., Estévez, A. & Gil, A.J. (2019) How much Nubia-Eurasia convergence is accommodated by the NE end of the Eastern Betic Shear Zone (SE Spain)? Constraints from GPS Velocities. *Tectonics*, 38, 1824–1839.
- Brachert, T.C., Krautworst, U.M.R. & Stueckrad, M. (2002) Tectono-climatic evolution of a Neogene intramontane basin (Late Miocene Carboneras subbasin, southeast Spain): revelations from basin mapping and biofacies analysis. *Basin Research*, 14, 503–521.
- Bradley, R.W. & Venditti, J.G. (2017) Reevaluating dune scaling relations. *Earth-Science Reviews*, 165, 356–376.
- Braga, J.C., Martín, J.M. & Wood, J.L. (2001) Submarine lobes and feeder channels of redeposited, temperate carbonate and mixed siliciclastic-carbonate platform deposits (Vera Basin, Almería, southern Spain). *Sedimentology*, 48, 99–116.
- Braga, J.C., Martín, J.M. & Quesada, C. (2003) Patterns and average rates of late Neogene–Recent uplift of the Betic Cordillera, SE Spain. *Geomorphology*, 50, 3–26.
- Braga, J.C., Martín, J.M., Aguirre, J., Baird, C.D., Grunnaleite, I., Jensen, N.B., Puga-Bernabéu, A., Sælen, G. & Talbot, M.R. (2010) Middle-Miocene (Serravallian) temperate carbonates in a seaway connecting the Atlantic Ocean and the Mediterranean Sea (North Betic Strait, S Spain). *Sedimentary Geology*, 225, 19–33.
- Bressan, G.S., Kietzmann, D.A. & Palma, R.M. (2013) Facies analysis of a Toarcian Bajocian shallow marine/coastal succession (Bardas Blancas Formation) in northern Neuquén Basin, Mendoza province, Argentina. *Journal of South American Earth Sciences*, 43, 112–126.
- Capella, W., Barhoun, N., Flecker, R., Hilgen, F.J., Kouwenhoven, T., Matenco, L.C., Sierro, F.J., Tulbure, M.A., Yousfi, M.Z. & Krijgsman, W. (2018) Palaeogeographic evolution of the late Miocene Rifian Corridor (Morocco): reconstructions from surface and subsurface data. *Earth-Science Reviews*, 180, 37–59.
- Cavazza, W. & Longhitano, S.G. (2022) Palaeostrait tectosedimentary facies during late Cenozoic microplate rifting and dispersal in the western Mediterranean. In: Rossi, V.M., Longhitano, S.G., Olariu, C. & Chiocci, F.L. (Eds.) *Straits and seaways: controls, processes and implications in modern and ancient systems*, Vol. 523. London: Geological Society, London, Special Publications, pp. 399–426.
- Chiarella, D. (2016) Angular and tangential toset geometry in tidal cross-strata: an additional feature of current-modulated deposits. In: Tessier, B. & Reynaud, J.-Y. (Eds.) *Contributions to modern and ancient tidal sedimentology: proceedings of the tidalites 2012 conference*, Vol. 47. Oxford: Wiley-Blackwell, International Association of Sedimentologists, Special Publication, pp. 191–201.
- Chiarella, D. & Longhitano, S.G. (2012) Distinguishing depositional environments in shallow-water mixed bio-siliciclastic deposits on the basis of the degree of heterolithic segregation (Gelasian, Southern Italy). *Journal of Sedimentary Research*, 82, 969–990.
- Chiarella, D., Longhitano, S.G. & Muto, F. (2012) Sedimentary features of the Lower Pleistocene mixed siliciclastic-bioclastic tidal deposits of the Catanzaro Strait (Calabrian Arc, south Italy). *Rendiconti Online della Società Geologica Italiana*, 21, 919–920.
- Chiarella, D., Longhitano, S.G. & Tropeano, M. (2017) Types of mixing and heterogeneities in siliciclastic-carbonate sediments. *Marine and Petroleum Geology*, 88, 617–637.
- Chiarella, D., Capella, W., Longhitano, S.G. & Muto, F. (2020) Fault-controlled base-of-scarp deposits. *Basin Research*, 33, 1056–1075.
- Coletti, G., Bosio, G., Collareta, A., Buckeridge, J., Consani, S. & El Kateb, A. (2018) Palaeoenvironmental analysis of the Miocene barnacle facies: case studies from Europe and South America. *Geologica Carpathica*, 69, 573–592.
- Dabrio, C.J. (1987) Las sand waves calcareníticas del río Alías (Mioplioceno de la Cuenca de Níjar, Almería). *Acta Geologica Hispánica*, 22, 159–166.
- Dabrio, C.J., Esteban, M. & Martín, J.M. (1981) The coral reef of Níjar (Uppermost Miocene), Almería Province, SE Spain. *Journal of Sedimentary Research*, 51, 521–539.
- Dalrymple, R.W., Zaitlin, B.A. & Boyd, R. (1992) Estuarine facies models: conceptual basis and stratigraphic implications. *Journal of Sedimentary Research*, 62, 1130–1146.
- Dalrymple, R.W. (2023) A review of the morphology, physical processes and deposits of modern straits. In: Rossi, V.M.,

- Longhitano, S.G., Olariu, C. & Chiocci, F.L. (Eds.) *Straits and seaways: controls, processes and implications in modern and ancient systems*, Vol. 523. London: Geological Society, London, Special Publications, pp. 17–83.
- Davis, R.A., Jr. (2012) Tidal signatures and their preservation potential in stratigraphic sequences. In: Davis, R.A., Jr. & Dalrymple, R.W. (Eds.) *Principles of tidal sedimentology*. Dordrecht: Springer Science+Business Media, pp. 35–55.
- Dewey, J.F., Helman, M.L., Turco, E., Hutton, D.H.W. & Knott, S.D. (1989) Kinematics of the western Mediterranean. In: Coward, M.P., Dietrich, D. & Park, R.G. (Eds.) *Alpine tectonics*, Vol. 45. London: Geological Society, London, Special Publications, pp. 265–283.
- Dosser, H.V., Waterman, S., Jackson, J.M., Hannah, C.G., Evans, W. & Hunt, B.P.V. (2021) Stark physical and biogeochemical differences and implications for ecosystem stressors in the Northeast Pacific coastal ocean. *Journal of Geophysical Research: Oceans*, 126, e2020JC017033. <https://doi.org/10.1029/2020JC017033>
- Echeverría, A., Khazaradze, G., Asensio, E. & Masana, E. (2015) Geodetic evidence for continuing tectonic activity of the Carboneras fault (SE Spain). *Tectonophysics*, 663, 302–309.
- Emmel, F.J. & Curran, J.R. (1982) A submerged Late Pleistocene delta and other features related to sea level changes in the Malacca Strait. *Marine Geology*, 47, 197–216.
- Ercilla, G., Galindo-Zaldívar, J., Estrada, F., Valencia, J., Juan, C., Casas, D., Alonso, B., Comas, M.C., Tendero-Salmerón, V., Casalbore, D., Azpiroz-Zabala, M., Bárcenas, P., Ceramicola, S., Chiocci, F.L., Idárraga-García, J., López-González, N., Mata, P., Palomino, D., Rodríguez-García, J.A., Teixeira, M., Nespereira, J., Vázquez, J.T. & Yenes, M. (2022) Understanding the complex geomorphology of a deep sea area affected by continental tectonic indentation: the case of the Gulf of Vera (Western Mediterranean). *Geomorphology*, 208, 108126.
- Ferrarin, C., Bellafiore, D., Sannino, G., Bajo, M. & Umgiesser, G. (2018) Tidal dynamics in the inter-connected Mediterranean, Marmara, Black and Azov seas. *Progress in Oceanography*, 161, 102–115.
- Fortuin, A.R. & Krijgsman, W. (2003) The Messinian of the Nijar Basin (SE Spain): sedimentation, depositional environments and paleogeographic evolution. *Sedimentary Geology*, 160, 213–242.
- Gardner, K. & Dorsey, R.J. (2021) Mixed carbonate–siliciclastic sedimentation at the margin of a late Miocene tidal strait, lower Colorado River Valley, south-western USA. *Sedimentology*, 68, 1893–1922.
- Galindo-Zaldívar, J., Braga, J.C., Marín-Lechado, C., Ercilla, G., Martín, J.M., Pedrera, A., Casas, D., Aguirre, J., Ruiz-Constán, A., Estrada, F., Puga-Bernabéu, Á., Sanz de Galdeano, C., Juan, C., García-Alix, A., Vázquez, J.T. & Alonso, B. (2019) Extension in the Western Mediterranean. In: Quesada, C. & Oliveira, J.T. (Eds.) *The geology of Iberia: a geodynamic approach: volume 4: Cenozoic basins*. Cham: Springer International Publishing, pp. 61–103.
- Gattolin, G., Breda, A. & Preto, N. (2013) Demise of Late Triassic carbonate platforms triggered the onset of a tide-dominated depositional system in the Dolomites, Northern Italy. *Sedimentary Geology*, 297, 38–49.
- Giaconia, F., Booth-Rea, G., Martínez-Martínez, J.M., Azañón, J.M. & Pérez-Peña, J.V. (2012) Geomorphic analysis of the Sierra Cabrera, an active pop-up in the constrictional domain of conjugate strike-slip faults: the Palomares and Polopos fault zones (eastern Betics, SE Spain). *Tectonophysics*, 580, 27–42.
- Giaconia, F., Booth-Rea, G., Martínez-Martínez, J.M., Azañón, J.M., Storti, F. & Artoni, A. (2014) Heterogeneous extension and the role of transfer faults in the development of the southeastern Betic basins (SE Spain). *Tectonics*, 33, 2467–2489.
- Göktaşan, E., Ergin, M., Özyalvaç, M., Sur, H.I., Tur, H., Görüm, T., Ustaömer, T., Batuk, F.G., Alp, H., Birkan, H., Türker, A., Gezgin, E. & Özturan, M. (2008) Factors controlling the morphological evolution of the Çanakkale Strait (Dardanelles, Turkey). *Geo-Marine Letters*, 28, 107–129.
- Gupta, S. & Allen, P.A. (1999) Fossil shore platforms and drowned gravel beaches: evidence for high-frequency sea-level fluctuations in the distal Alpine foreland basin. *Journal of Sedimentary Research*, 69, 394–413.
- Harvey, A. & Mather, A. (2015) *Classic geology in Europe 12, Almeria*. Dunedin: Edinburgh.
- Hodgetts, D., Gawthorpe, R.L., Wilson, P. & Rarity, F. (2007) Integrating Digital and Traditional Field Techniques Using Virtual Reality Geological Studio (VRGS). 69th EAGE Conference and Exhibition incorporating SPE EUROPEC 2007.
- Hsü, K.J., Montadert, L., Bernouilli, D., Cita, M.B., Erikson, A., Garrison, R.G., Kidd, R.B., Mélières, F., Müller, C. & Wright, R. (1977) History of the Mediterranean salinity crisis. *Nature*, 267, 399–403.
- Ikehara, K. & Kinoshita, Y. (1994) Distribution and origin of subaqueous dunes on the shelf of Japan. *Marine Geology*, 120, 75–87.
- James, N.P., Seibel, M.J., Dalrymple, R.W., Besson, D. & Parize, O. (2014) Warm-temperate, marine, carbonate sedimentation in an Early Miocene, tide-influenced, incised valley; Provence, south-east France. *Sedimentology*, 61, 497–534.
- Keller, G.H. & Richards, A.F. (1967) Sediments of the Malacca Strait, Southeast Asia. *Journal of Sedimentary Petrology*, 37, 102–127.
- Keller, J.V., Hall, S.H., Dart, C.J. & McClay, K.R. (1995) The geometry and evolution of a transpressional strike-slip system: the Carboneras Fault, SE Spain. *Journal of the Geological Society*, 152, 339–351.
- Koulali, A., Ouazar, D., Tahayt, A., King, R.W., Vernant, P., Reilinger, R.E., McClusky, S., Mourabit, T., Davila, J.M. & Amraoui, N. (2011) New GPS constraints on active deformation along the Africa–Iberia plate boundary. *Earth and Planetary Science Letters*, 308, 211–217.
- Kranck, K. (1972) Geomorphological development and post-Pleistocene sea-level changes, Northumberland Strait, Maritime Provinces. *Canadian Journal of Earth Sciences*, 9, 835–844.
- Krautworst, U.M.R. & Brachert, T.C. (2003) Sedimentary facies during early stages of flooding in an extensional basin: the Breche Rouge de Carboneras (Late Miocene, Almería/SE Spain). *International Journal of Earth Sciences (Geologische Rundschau)*, 92, 610–623.
- Longhitano, S.G. (2011) The record of tidal cycles in mixed siliciclastic deposits: examples from small Plio-Pleistocene peripheral basins of the microtidal Central Mediterranean Sea. *Sedimentology*, 58, 691–719.
- Longhitano, S.G. (2013) A facies-based depositional model for ancient and modern, tectonically-confined tidal straits. *Terra Nova*, 25, 446–452.
- Longhitano, S.G. (2018a) Between Scylla and Charybdis (part 1): the sedimentary dynamics of the modern Messina Strait (central

- Mediterranean) as analogue to interpret the past. *Earth-Science Reviews*, 185, 259–287.
- Longhitano, S.G. (2018b) Between Scylla and Charybdis (part 2): the sedimentary dynamics of the ancient, Early Pleistocene Messina Strait (central Mediterranean) based on its modern analogue. *Earth-Science Reviews*, 179, 248–286.
- Longhitano, S.G. & Steel, R.J. (2016) Deflection of the progradational axis and asymmetry in tidal seaway and strait deltas: insights from two outcrop case studies. In: Hampson, G.J., Reynolds, A.D., Bedley, B.K. & Wells, M.R. (Eds.) *Sedimentology of paralic reservoirs: recent advances*, Vol. 444. London: Geological Society, Special Publication, pp. 141–172.
- Longhitano, S.G. & Chiarella, D. (2020) Tidal straits: basic criteria for recognizing ancient tidal straits from the rock record. In: Scarselli, N., Adam, J. & Chiarella, D. (Eds.) *Regional Geology and Tectonics*, 2nd edition, Chapter 15. Cham: Elsevier, pp. 365–415.
- Longhitano, S.G., Sabato, L., Tropeano, M. & Gallicchio, S. (2010) A mixed bioclastic–siliciclastic flood-tidal delta in a micro tidal setting: depositional architectures and hierarchical internal organization (Pliocene, southern Apennine, Italy). *Journal of Sedimentary Research*, 80, 36–53.
- Longhitano, S.G., Chiarella, D., Di Stefano, A., Messina, C., Sabato, L. & Tropeano, M. (2012) Tidal signatures in Neogene to Quaternary mixed deposits of southern Italy straits and bays. *Sedimentary Geology*, 279, 74–96.
- Longhitano, S.G., Chiarella, D. & Muto, F. (2014) Three-dimensional to two-dimensional cross-strata transition in the lower Pleistocene Catanzaro tidal strait transgressive succession (southern Italy). *Sedimentology*, 61, 2136–2171.
- Longhitano, S.G., Chiarella, D., Gugliotta, M. & Ventra, D. (2021) Coarse-grained deltas approaching shallow-water canyon heads: a case study from the Lower Pleistocene Messina Strait, Southern Italy. *Sedimentology*, 68, 2523–2562.
- Martín, J.M., Braga, J.C., Betzler, C. & Brachert, T. (1996) Sedimentary model and high-frequency cyclicity in a Mediterranean, shallow-shelf, temperate-carbonate environment (uppermost Miocene, Agua Amarga Basin, Southern Spain). *Sedimentology*, 43, 263–277.
- Martín, J.M., Braga, J.C., Aguirre, J. & Betzler, C. (2004) Contrasting models of temperate carbonate sedimentation in a small Mediterranean embayment: the Pliocene Carboneras Basin, SE Spain. *Journal of the Geological Society of London*, 161, 387–399.
- Martín, J.M., Braga, J.C. & Betzler, C. (2001) The Messinian Guadalhorce corridor: the last northern, Atlantic–Mediterranean gateway. *Terra Nova*, 13, 418–424.
- Martín, J.M., Braga, J.C. & Betzler, C. (2003) Late Neogene–recent uplift of the Cabo de Gata volcanic province, Almería, SE Spain. *Geomorphology*, 50, 27–42.
- Martín, J.M., Braga, J.C., Aguirre, J. & Puga-Bernabéu, Á. (2009) History and evolution of the North-Betic Strait (Prebetic Zone, Betic Cordillera): a narrow, early Tortonian, tidal-dominated, Atlantic–Mediterranean marine passage. *Sedimentary Geology*, 216, 80–90.
- Martín, J.M., Puga-Bernabéu, Á., Aguirre, J. & Braga, J.C. (2014) Miocene Atlantic-Mediterranean seaways in the Betic Cordillera (Southern Spain). *Revista de la Sociedad Geológica de España*, 27, 175–186.
- Masana, E., Moreno, X., Gràcia, E., Pallàs, R., Ortuño, M., López, R., Gómez-Novell, O., Ruano, P., Perea, H., Stepancikova, P. & Khazaradze, G. (2018) First evidence of paleoearthquakes along the Carboneras Fault Zone (SE Iberian peninsula): Los Trances site. *Geologica Acta*, 16, 461–476.
- Miller, K.G., Kominz, M.A., Browning, J.V., Wright, J.D., Mountain, G.S., Katz, M.E., Sugarman, P.J., Cramer, B.S., Christie-Blick, N. & Pekar, S.F. (2005) The Phanerozoic record of global sea-level change. *Science*, 310, 1293–1298.
- Mitchell, N.C., Huthnance, J.M., Schmitt, T. & Todd, B. (2013) Threshold of erosion of submarine bedrock landscapes by tidal currents. *Earth Surface Processes and Landforms*, 38, 627–639.
- Molina, R., Manno, G., Lo Re, C., Anfuso, G. & Ciralo, G. (2019) Storm energy flux characterization along the Mediterranean coast of Andalusia (Spain). *Water*, 11, 509.
- Montenat, C. (1990) Les Bassins Néogènes du Domaine Bétique Orientale (Espagne): tectonique et Sédimentation dans un Couloir de Décrochement. *Documents et Travaux de l'IGAL*, 12–13, 392.
- Montenat, C., Ott d'Estevou, P., Leyrit, H. & Barrier, P. (2000) The Brèche rouge of Carboneras. An example of late Miocene volcanic megabreccia deposited in a deep-marine basin controlled by wrench tectonics (Eastern Betics, Spain). In: Leyrit, H. & Montenat, C. (Eds.) *Volcaniclastic rocks from magmas to sediments*. Boca Raton, FL: CRC Press, pp. 193–215.
- Moreno, X., Masana, E., Pallàs, R., Gràcia, E., Rodés, A. & Bordonau, J. (2015) Quaternary tectonic activity of the Carboneras fault in the La Serrata range (SE Iberia): geomorphological and chronological constraints. *Tectonophysics*, 663, 78–94.
- O'Connell, B., Dorsey, R.J., Hasiotis, S. & Hood, A. (2021) Mixed carbonate-siliciclastic tidal sedimentation in the Miocene to Pliocene Bouse Formation, palaeo-Gulf of California. *Sedimentology*, 68, 1028–1068.
- Olariu, C., Steel, R.J., Dalrymple, R.W. & Gingras, M.K. (2012) Tidal dunes v. tidal bars: the sedimentological and architectural characteristics of compound dunes in a tidal seaway, the lower Baronia Sandstone (Lower Eocene), Ager Basin, Spain. *Sedimentary Geology*, 279, 134–155.
- Omodeo Salé, S., Gennari, R., Lugli, S., Manzi, V. & Roveri, M. (2012) Tectonic and climatic control on the Late Messinian sedimentary evolution of the Nijar Basin (Betic Cordillera, Southern Spain). *Basin Research*, 24, 314–337.
- Pedraza, A., Marín-Lechado, C., Galindo-Zaldívar, J., Rodríguez-Fernández, L.R. & Ruiz-Constán, A. (2006) Fault and fold interaction during the development of the Neogene-Quaternary Almería-Nijar basin (SE Betic Cordilleras). In: Moratti, G. & Chalouan, A. (Eds.) *Tectonics of the Western Mediterranean and North Africa*, Vol. 262. London: Geological Society, London, Special Publications, pp. 217–230.
- Pedraza, A., Mancilla, F., Ruiz-Constán, A., Galindo-Zaldívar, J., Morales, J., Arzate, J., Marín-Lechado, C., Ruano, P., Buontempo, L., Anahnah, F. & Stich, D. (2010) Crustal-scale transcurrent fault development in a weak-layered crust from an integrated geophysical research: Carboneras Fault Zone, eastern Betic Cordillera, Spain. *Geochemistry, Geophysics, Geosystems*, 11(12), Q12005.
- Proctor, R. & Carter, L. (1989) Tidal and sedimentary response to the Late Quaternary closure and opening of Cook Strait, New Zealand: results from numerical modeling. *Paleoceanography*, 4, 167–180.
- Puga-Bernabéu, Á., Braga, J.C., Aguirre, J. & Martín, J.M. (2022) Sedimentary dynamics and topographic controls on the

- tidal-dominated Zagra Strait, Early Tortonian, Betic Cordillera, Spain. In: Rossi, V.M., Longhitano, S.G., Olariu, C. & Chiocci, F.L. (Eds.) *Straits and seaways: controls, processes and implications in modern and ancient systems*, Vol. 523. London: Geological Society, London, Special Publications, pp. 427–451.
- Reynaud, J.-Y. & Dalrymple, R.W. (2012) Shallow-marine tidal deposits. In: Davis, R.A., Jr. & Dalrymple, B.W. (Eds.) *Principles of tidal sedimentology*. New York: Springer, pp. 335–370.
- Reynaud, J.-Y., Dalrymple, R.W., Vennin, E., Parize, O., Besson, D. & Rubino, J.-L. (2006) Topographic controls on production and deposition of tidal cool-water carbonates, Uzès Basin, SE France. *Journal of Sedimentary Research*, 76, 117–130.
- Reynaud, J.-Y., Ferrandini, M., Ferrandini, J., Santiago, M., Thion, I., André, J.-P., Barthet, Y., Guennoc, P. & Tessier, B. (2013) From non-tidal shelf to tide-dominated strait: the Miocene Bonifacio Basin, Southern Corsica. *Sedimentology*, 60, 599–623.
- Roberts, M.J., Scourse, J.D., Bennell, J.D., Huws, D.G., Jago, C.F. & Long, B.T. (2011) Late Devonian and Holocene relative sea-level change in North Wales, UK. *Journal of Quaternary Science*, 26, 141–155.
- Rohling, E.J., Foster, G.L., Grant, K.M., Marino, G., Roberts, A.P., Tamisiea, M.E. & Williams, F. (2014) Sea-level and deep-sea-temperature variability over the past 5.3 million years. *Nature*, 508, 477–482.
- Rondeel, H.E. (1965) Geological investigations in the western Sierra Cabrera. PhD Thesis, University of Amsterdam, The Netherlands.
- Rosenbaum, G., Lister, G.S. & Duboz, C. (2002) Relative motions of Africa, Iberia and Europe during Alpine orogeny. *Tectonophysics*, 359, 117–129.
- Rossi, V.M., Longhitano, S.G., Mellere, D., Dalrymple, R.W., Steel, R.J., Chiarella, D. & Olariu, C. (2017) Interplay of tidal and fluvial processes in an early Pleistocene, delta-fed, strait margin (Calabria, Southern Italy). *Marine and Petroleum Geology*, 87, 14–30.
- Rossi, V.M., Longhitano, S.G., Olariu, C. & Chiocci, F.L. (Eds.). (2023a) About this title—straits and seaways: controls, processes and implications in modern and ancient systems. In: *Straits and seaways: controls, processes and implications in modern and ancient systems*. London: Geological Society, London, Special Publications, p. 523.
- Rossi, V.M., Longhitano, S.G., Olariu, C. & Chiocci, F.L. (2023b) Straits and seaways: end members within the continuous spectrum of the dynamic connection between basins. In: Rossi, V.M., Longhitano, S.G., Olariu, C. & Chiocci, F.L. (Eds.) *Straits and seaways: controls, processes and implications in modern and ancient systems*, Vol. 523. London: Geological Society, London, Special Publications, pp. 85–109.
- Rouchy, J.M. & Caruso, A. (2006) The Messinian salinity crisis in the Mediterranean basin: a reassessment of the data and an integrated scenario. *Sedimentary Geology*, 188–189, 35–67.
- Rutter, E.H., Faulkner, D.R. & Burgess, R. (2012) Structure and geological history of the Carboneras Fault Zone, SE Spain: part of a stretching transform fault system. *Journal of Structural Geology*, 45, 68–86.
- Rutter, E.H., Burgess, R. & Faulkner, D.R. (2014) Constraints on the movement history of the Carboneras Fault Zone (SE Spain) from stratigraphy and  $^{40}\text{Ar}$ – $^{39}\text{Ar}$  dating of Neogene volcanic rocks. *Geological Society, London, Special Publications*, 394, 79–99.
- Sanz de Galdeano, C. (1990) Geologic evolution of the Betic Cordilleras in the Western Mediterranean, Miocene to the present. *Tectonophysics*, 172, 107–119.
- Schmidt, G. & Seyfried, H. (1991) Depositional sequences and sequence boundaries in fore-arc coastal embayments: case histories from Central America. In: Macdonald, D.I.M. (Ed.) *Sedimentation, tectonics and Eustasy: Sea-level changes at active plate margins*, Vol. 12. Oxford: Blackwell Scientific Publisher, International Association of Sedimentologists Special Publication, pp. 241–258.
- Scotney, P., Burgess, R. & Rutter, E.H. (2000)  $^{40}\text{Ar}$ / $^{39}\text{Ar}$  age of the Cabo de Gata volcanic series and displacements on the Carboneras fault zone, SE Spain. *Journal of the Geological Society*, 157, 1003–1008.
- Semeniuk, V. & Johnson, D.P. (1985) Modern and Pleistocene rocky shore sequences along carbonate coastlines, southwestern Australia. *Sedimentary Geology*, 44, 225–261.
- Serpelloni, E., Vannucci, G., Pondrelli, S., Argnani, A., Casula, G., Anzidei, M., Baldi, P. & Gasperini, P. (2007) Kinematics of the Western Africa-Eurasia plate boundary from focal mechanisms and GPS data. *Geophysical Journal International*, 169, 1180–1200.
- Serrano, F. (1990) El Mioceno medio en el área de Níjar (Almería, España). *Revista de la Sociedad Geológica de España*, 3, 65–77.
- Serrano, F. (1992) Biostratigraphic control of Neogene volcanism in Sierra de Gata (south-east Spain). *Geologie en Mijnbouw*, 71, 3–14.
- Shaw, J., Todd, B.J., Li, M.Z. & Wu, Y. (2012) Anatomy of the tidal scour system at Minas Passage, Bay of Fundy, Canada. *Marine Geology*, 323–325, 123–134.
- Sola, F., Puga-Bernabéu, Á., Aguirre, A. & Braga, J.C. (2017) Heterozoan carbonate deposition on a steep basement escarpment (Late Miocene, Almería, south-east Spain). *Sedimentology*, 64, 1107–1131.
- Sola, F., Braga, J.C. & Saelen, G. (2022) Contradictory coeval vertical facies changes in upper Miocene heterozoan carbonate–terrigenous deposits (Sierra de Gádor, Almería, SE Spain). *Journal of Sedimentary Research*, 92, 257–274.
- Telesca, D., Longhitano, S.G., Pistis, M., Pascucci, V., Tropeano, M. & Sabato, L. (2020) Sedimentology of a transgressive middle-upper Miocene succession filling a tectonically confined, current dominated seaway (the Logudoro Basin, northern Sardinia, Italy). *Sedimentary Geology*, 400, 105626.
- Weijermars, R. (1991) Geology and tectonics of the Betic Zone, SE Spain. *Earth Science Reviews*, 31, 153–236.
- Yalin, M.S. (1964) Geometrical properties of sand waves. *Journal of the Hydraulics Division*, 90, 105–119.

**How to cite this article:** Sola, F., Puga-Bernabéu, Á. & Braga, J.C. (2024) Tidally influenced deposits in the Río Alías Strait connecting a marginal basin with the Mediterranean Sea (Pliocene, South-East Spain). *The Depositional Record*, 00, 1–30. Available from: <https://doi.org/10.1002/dep2.303>